COO-3065-152

CONF-760874--1

~~UR-152~~

HADRON PHYSICS AT FERMILAB

BY

T. FERBEL

THE UNIVERSITY OF ROCHESTER

DEPARTMENT OF PHYSICS AND ASTRONOMY

ROCHESTER , NEW YORK

42 attached

DISCLAIMER

UR-587 COO-3065-152

HADRON PHYSICS AT FERMILAB*

T. Ferbel

Department of Physics and Astronomy

University of Rochester, Rochester, New York, 14627 USA

ABSTRACT

I survey recent experimental results from studies of hadron interactions at Fermilab. Elastic, total and charge-exchange cross section measurements, diffractive phenomena, and inclusive production, using nuclear as well as hydrogen targets, are discussed in these lectures.

INTRODUCTION

The momentous J/ψ discoveries of almost two years ago [1] have put an unusually depressing damper on the entire field of "old-fashioned" hadron physics. Subsequent to the J/ψ announcements, every able-bodied experimentalist who had equipment installed on the experimental floor of Fermilab abandoned all his previous well-planned efforts to join in the mad search for charm, color or what have you. (Unless your experiment involves a prompt lepton trigger or has such key words as "search for narrow.." on the proposal, you are still regarded in some circles of Fermilab as a myopic pariah.) Despite all the frenetic J/ψ related activity, several groups have nevertheless managed to generate some outstanding results on "hard-core" hadron physics. In these lectures I will summarize some recent experimental and phenomenological investigations which I find particularly stimulating. I will try, where possible, to present those results which tend to raise new questions rather than answer old ones.

*Research supported by the United States Energy Research and Development Administration, under contract number E(11-1)-3065.

August 30, 1976.

These lectures are to appear in the Proceedings of the E. Majorana School of Subnuclear Physics (Erice-1976), A. Zichichi, ed.

I. TOTAL, ELASTIC AND CHARGE-EXCHANGE CROSS SECTIONS

Total Cross Sections

Precision measurements of total and of elastic scattering cross sections are now available for $K^{\pm}$, $\pi^{\pm}$, n, p and $\bar{p}$ projectiles. The latest data for total cross sections have recently been published [2]. I reproduce the results of these measurements on hydrogen and deuterium in Fig. 1. It is clear that all hadronic total cross sections appear to fall from values measured at lower energies; after passing broad minima, which occur near $\sim$10 GeV/c for K^+p and perhaps as high as $\sim$300 GeV/c for $\bar{p}p$ (no $\bar{p}p$ measurements are as yet available above 200 GeV/c!), the cross sections start to rise again. The differences between antiparticle-nucleon and particle-nucleon cross sections shown in Fig. 2 can be parameterized as a function of the square of the energy in the center of mass (s) in terms of a power-law dependence of the form $As^{\alpha-1}$. The values of α obtained from a fit to the difference in the $\bar{p}p$ and pp cross-section (α_{pp}=0.39±0.02) and for the K^-p and K^+p difference (α_{Kp} = 0.40 ± 0.04) are the same within error. From Regge phenomenology we expect these differences in the particle-antiparticle cross sections to isolate the dominant contribution of the ω Regge trajectory (although the differences also contain ρ and A_2 terms, these mesons do not couple nearly as strongly to the proton as the ω does). Recent measurements of K_S^0 regeneration on carbon [3] yield a value for the ω trajectory at t=0 of $\alpha_\omega(t=0)=0.43\pm0.01$, a result in good agreement with the above given α_{pp} and α_{Kp}. Similarly, the value of $\alpha_{\pi p}=0.55\pm0.03$, obtained from the data in Fig. 2, is reasonably consistent with that expected from the contribution of the ρ trajectory to the difference between the π^-p and the π^+p cross section. (A value of $\alpha_\rho(0)=0.48\pm0.04$ has recently been extracted from measurements of $\pi^-p \to \pi^0 n$ at Fermilab [4].)

The data in Fig. 2 indicate that $\Delta\sigma_T(p^{\pm}p)$ is about 2-3 times larger than $\Delta\sigma_T(K^{\pm}p)$; also, $\Delta\sigma_T(p^{\pm}n)$ is about 4 times larger than $\Delta\sigma_T(K^{\pm}n)$. These kind of differences in the hadron-hadron cross sections can be used to test various symmetry relations. In particular, the ratio $3[\Delta\sigma(K^{\pm}p)+\Delta\sigma(K^{\pm}n)]/[\Delta\sigma(p^{\pm}p)+\Delta\sigma(p^{\pm}n)]$ measures the contribution of ω-exchange to kaon-nucleon relative to baryon-nucleon total cross sections. The constancy observed for this ratio from $\sim$15 GeV/c through 200 GeV/c speaks for an energy-independent universal coupling of the ω meson to kaons and baryons. I will not elaborate further on this subject, I will note only in passing that, besides ω universality, ρ-ω universality and the Johnson-Treiman relations are all in agreement with the data, to $\sim$(10-20)% accuracy, in the 30-250 GeV/c momentum range. (These agreements may be short-lived if the trend observed for the

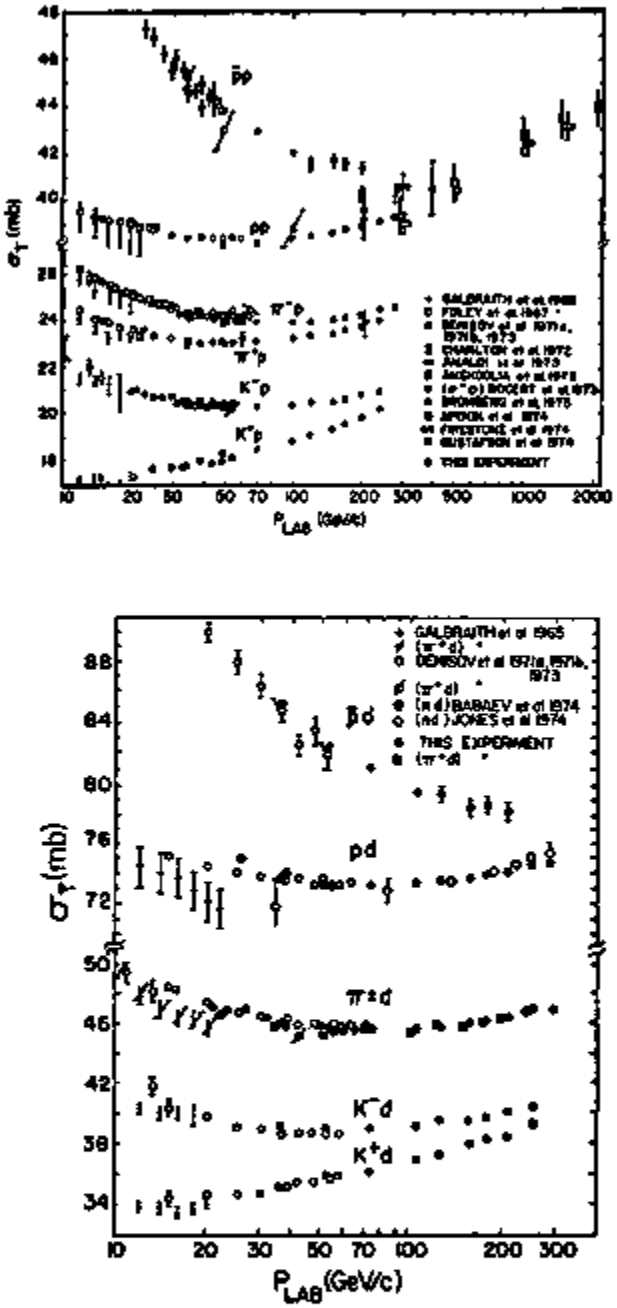

Figure 1: Total cross sections for hadron interactions with hydrogen and deuterium target particles.

K^-p-K^+p difference to decrease more rapidly for momenta above 100 GeV/c persists with further increase in energy or in data!)

The last item I will discuss in this section is a compilation by Whitmore [5] of the total $\bar{p}p$ meson-annihilation cross section as a function of laboratory momentum. Figure 3 displays the energy dependence of this cross section in comparison to the difference of the $\bar{p}p$ and pp total cross sections. It is interesting that the $s^{\alpha_{pp}-1}$ form given in Fig.2 also appears to describe the meson annihilation cross section. An energy variation of just this sort was, in fact, predicted recently by Eylon and Harari [6] on the basis of a duality-diagram model. The implication of the constancy of $\Delta\sigma/\sigma(\bar{p}p \to \text{mesons})$ according to Eylon and Harari, is that $\bar{p}p$ annihilations contribute through the unitarity relation to the Pomeranchukon rather than to the meson exchange terms in the $\bar{p}p$ total cross section. The surprising (and perhaps accidental) result of Fig. 3 is that the meson annihilation cross section agrees in magnitude with $\Delta\sigma$ (Eylon and Harari predict that as s increases $\Delta\sigma/\sigma(\bar{p}p \to \text{mesons})$ approaches a constant ≤ 1). To put these results in some perspective, I remind you that at $\sim$5 GeV/c, for example, the difference in the $\bar{p}p$ and pp elastic cross section is $\sim$5 mb, which means that the $\bar{p}p$ inelastic non-annihilation cross section is smaller than

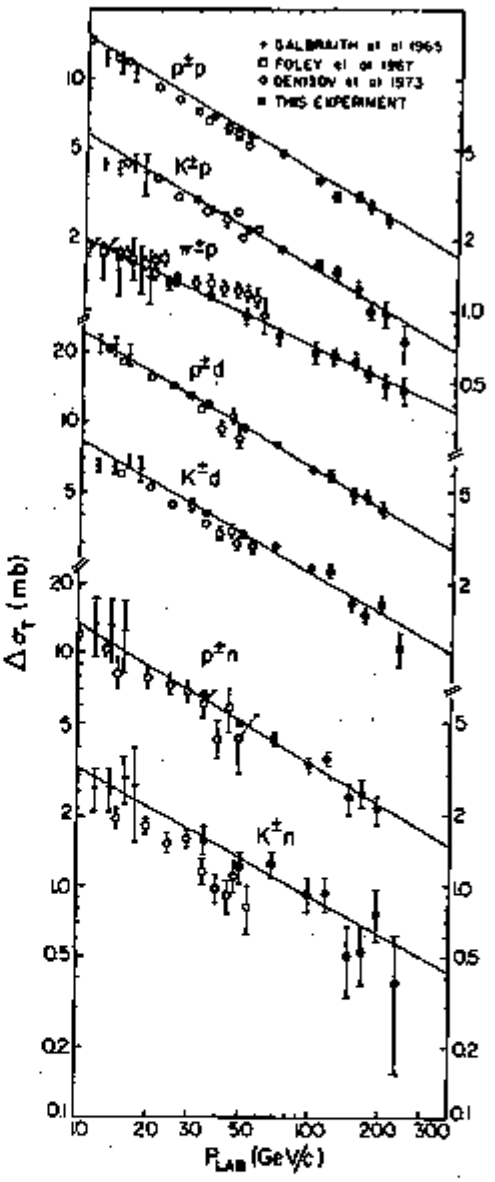

Figure 2: Differences in hadron-nucleon and antihadron-nucleon total cross sections as a function of incident momentum in the laboratory.

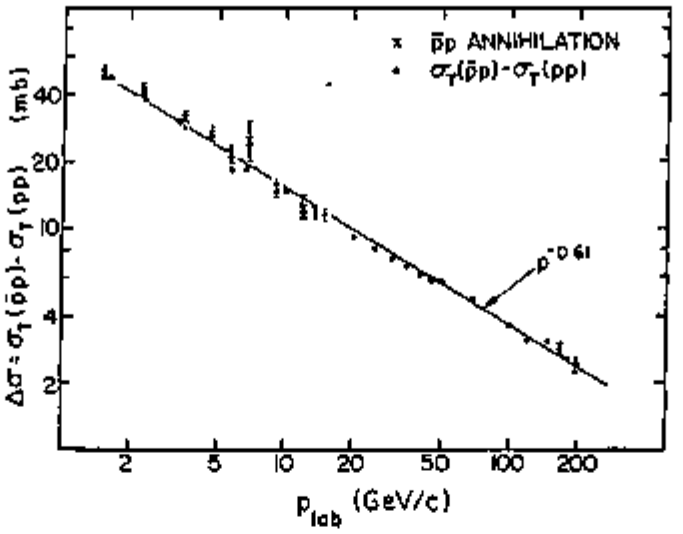

Figure 3: Comparison of the difference in $\bar{p}p$ and pp total cross sections with the cross section for $\bar{p}p$ annihilation into mesons.

the inelastic pp cross section, and so it is clearly not proper to regard the $\bar{p}p$ interaction as simply the super-position of the pp interaction and the additional annihilation channel which is not available to the pp system. Absorption effects in the final states certainly play an important role in the generation of $\Delta\sigma$; this is a theme I will periodically return to in the course of this lecture.

Elastic Scattering

Data on the elastic scattering of $\pi^{\pm}$, $K^{\pm}$ and $\bar{p}$ on hydrogen in the 50-200 GeV/c momentum range have become available during this past year. Figure 4 provides the character of the data obtained at small momentum transfers [7]. The differential cross sections for the scattering of particles on hydrogen are observed to have shapes similar to those found for the scattering of their respective antiparticles on hydrogen. All the differential cross sections appear to have curvature in t, and all except the $\bar{p}p$ channel tend to become steeper with increasing momentum (only the 100 GeV/c data are shown in Fig. 4). The latter result is emphasized in Fig. 5, where the slopes of the elastic spectra $B(t) = d(\ell n\, d\sigma/dt)/dt$ at $t=0.2$ GeV^2 are plotted as a function of s. The difference in the steepness of the K^+p and K^-p diffraction peaks, as well as of the $\bar{p}p$ and pp data, is slowly disappearing with increasing energy. All meson channels appear to be approaching a common value for B, a value which is substantially smaller than that describing the $\bar{p}p$ and pp slopes. At the smallest values

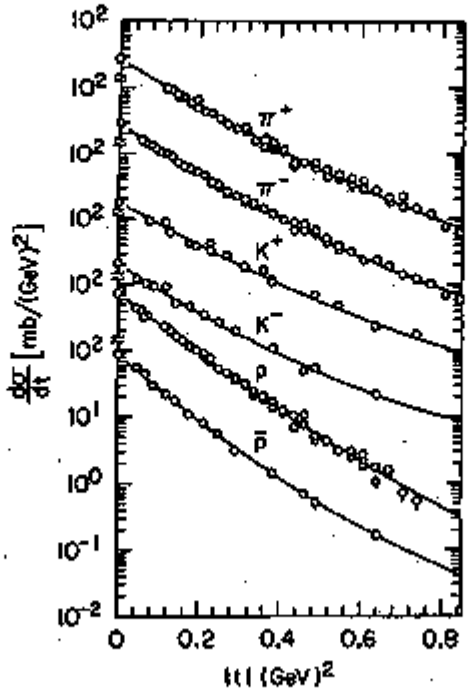

Figure 4: Elastic scattering differential cross section for hadrons incident on protons at 100 GeV/c.

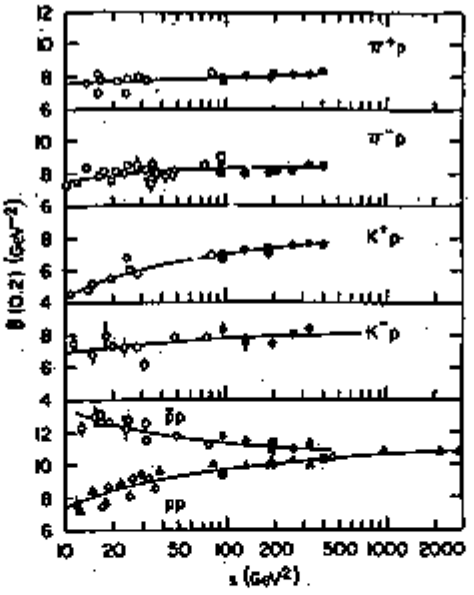

Figure 5: Slopes of the t-distributions at $|t|=0.2$ GeV^2 for hadron-proton and antihadron-proton elastic scattering as a function of s (see ref. 7).

of t, negative-particle cross sections tend to be larger than positive-particle cross sections, and vice versa at larger t. This effect, referred to as the crossover phenomenon, has been examined extensively at low energies [8].

In terms of a Regge-exchange picture, the observed difference between antiparticle and particle elastic scattering can be understood as follows. At small values of t the Pomeranchukon is the dominant exchange trajectory. The Pomeranchukon contribution to the elastic amplitude is mainly imaginary and non-flip. As in the case of total cross sections, the difference between antiparticle and particle elastic scattering can be attributed to the exchange of meson trajectories with negative charge conjugation. Consequently, the difference in elastic scattering must correspond to an interference term between the Pomeranchukon and the non-flip imaginary part of the relevant vector meson trajectories (Im $V_{\Delta\lambda=0}$). In the case of $K^{\pm}p$ and $p^{\pm}p$ the strongly coupled ω trajectory dominates the C=-1 exchange and the difference in K^-p and K^+p, as well as $\bar{p}p$ and pp, elastic scattering is therefore expected to be large. For the $\pi^{\pm}p$ channels, wherein ω cannot be exchanged because of the constraint of G-parity, only ρ contributes and consequently, because of the weak ρ-nucleon coupling, the (π^-p)-(π^+p) difference in elastic cross sections is expected to be small. The t-values at the positions of the cross overs are $t_c^K=0.19\pm0.04$ GeV^2 for $K^{\pm}p$ and $t_c^p=0.11\pm0.02$ GeV^2 for $p^{\pm}p$ data, in the momentum range 50-175 GeV/c [9]. There appears to be a weak energy dependence in t_c^p (t_c^p was measured to be 0.162 ± 0.004 GeV^2 near 5 GeV/c [8]). The latest data [9] pertaining to the cross-over phenomenon for $K^{\pm}p$ and $p^{\pm}p$ channels are shown in Fig. 6 in terms of the ratios $[(d\sigma/dt)^-/(d\sigma/dt)_f^+]$ and $[(d\sigma/dt)^+/(d\sigma/dt)_f^+]$, where $(d\sigma/dt)_f^+$ are the fitted (smoothed) data for positively charged projectiles.

The fact that t_c is so small means that $ImV_{\Delta\lambda=0}$ goes through zero for $t \lesssim 0.2$, which implies that the exchanged C=-1 contribution must be exceedingly peripheral. Davier and Harari [10] have, in fact, shown that within the framework of a dual absorption model the non-Pomeranchukon part of the elastic scattering amplitude is strongly dominated by the largest partial waves. (The Pomeranchuk contribution is central while the other Regge terms peak near an impact parameter of $\sim$1 fermi.) Consequently, these results suggest that a simple Regge-pole description of the crossover phenomenon cannot be adequate - strong absorption, cuts, or the like, are required to parameterize the effect.

For s-values above $\sim$25 GeV^2 the ratios of elastic to total cross sections appear to be constant and same (to within $\sim$5% accuracy) for antiparticles and particles [11]: $\pi^{\pm}p/K^{\pm}p/p^{\pm}p$ = 0.15/0.12/0.18. Similarly, the ratios of forward elastic slopes to total cross sections are energy independent [12]:0.34/0.39/0.26.

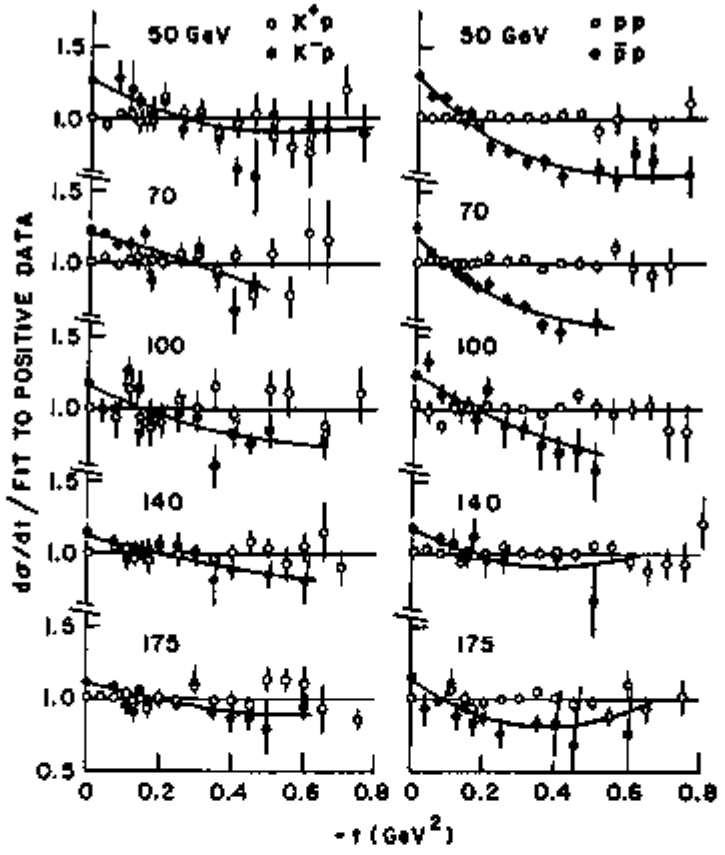

Figure 6: Study of the crossover phenomenon in elastic scattering between 50 GeV/c and 175 GeV/c.

The energy independence of these ratios can be realized in a model invoking geometrical scaling (GS) of the scattering amplitude in impact parameter (A(b,s)) [13]. The s-dependence in this model is contained entirely in the effective radius of the interaction (the scale), and the amplitude is energy independent when expressed in terms of b/R(s).[12,13] A pictorial way of viewing the GS assumption is that the distribution of nuclear matter does not change with s when it is parameterized in terms of the dimensionless quantity $\sqrt{\pi b^2/\sigma_{\text{inelastic}}}$. An immediate consequence of GS is that inelastic, elastic and total cross sections are proportional to R^2, as is the slope of the elastic differential cross sections at small t. Furthermore, because $d\sigma/dt$ can also be equated to $R^4|f_{el}(R^2t)|^2$, the quantity $(1/\sigma^2_{tot})(d\sigma/dt)$ should be s-independent

when plotted as a function of σ_{tot}·t. [14] All the above features of the GS hypothesis are in remarkable agreement with the data. Parameterizing a logarithmic growth of R^2 with increasing s also provides the observed rise in σ_{el}, σ_{tot} and B for the FNAL-ISR energy regime. Independent of the success of the GS hypothesis, it is clear that, phenomenologically, elastic scattering at small t is simplifying with increasing s-values.

A very surprising result in the pp elastic cross section at large t has been the rapid onset at 200 GeV/c of the Chou-Yang dip, observed previously at the ISR near $t = 1.5$ GeV^2 [15]. Figure 7 displays 100 GeV/c and 200 GeV/c pp data from Fermilab illustrating this unusual effect. The dip at 200 GeV/c occurs at t_D=1.5 GeV^2, which is to be compared with a value of $t_D \sim 1.3$ GeV^2 at 1500 GeV/c (ISR). An energy dependence of this kind for t_D is, again, consistent with the simple GS hypothesis.

Finally, preliminary measurements of the ratio of the real to imaginary part of the foward scattering amplitude (ρ), obtained using nuclear-coulomb interference at small t, for $\pi^{\pm}p$, $K^{\pm}p$ and $p^{\pm}p$ in the 70 GeV/c to 150 GeV/c range of incident momenta [16] appear to be in general agreement with the latest calculations [17] using dispersion relations and the new measurements of total cross sections [2]. The values of ρ are within $\sim$5% of zero near 100 GeV/c momentum, except for ρ_{pp}, which is ≈ -0.1, consistent with previous measurements [18] at Fermilab. The only sizeable discrepancy between the

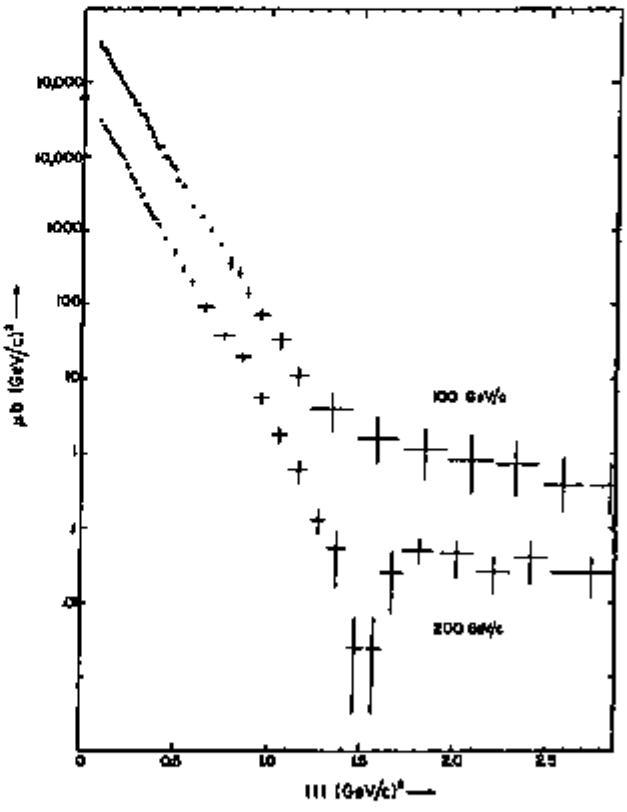

Figure 7: Elastic scattering cross sections for pp collisions at 100 GeV/c and 200 GeV/c.

new data and the calculations may be for the K^-p channel; however, the experimenters go out of their way to warn of the preliminary nature of their results.

Two-Body Charge-Exchange Reactions

Pion charge-exchange scattering has been measured at Fermilab in the π^- momentum range of 20 GeV/c to 200 GeV/c [4]. The differential cross sections and phenomenological fits to these spectra are shown in Fig. 8. The data display the well known helicity-flip turn-over at t=0 and the dip near t=0.5 GeV^2; these features have been attributed to the dominance of the ρ trajectory in the production. Although the authors point out that it is likely that the charge exchange amplitude has small contributions from sources other than just the ρ-trajectory (an asymmetry has been observed in the scattering from polarized targets near 5 GeV/c), they have nevertheless attempted to fit their data to the simple Regge-pole form $d\sigma/dt=\beta(t)\nu^{2\alpha(t)-2}$, where $\nu=(s-u)/4M$, u is the square of the four-momentum transfer between the incident π^- and the neutron, and M is the nucleon mass. The authors have performed a 7 parameter fit to β(t) and a 3 parameter fit to the effective trajectory $\alpha_\rho=\alpha_o+\alpha_1 t+\alpha_2 t^2$. The result of their fit to $\alpha_\rho(t)$ is displayed in Fig. 9. A straight line through points corresponding to ρ and g mesons falls remarkably close to the extracted α(t) for $|t|<0.3$ GeV^2. The value of $\alpha_\rho(0)$ is significantly lower than the value of 0.58±0.03 obtained at lower energies [19]. The relatively poor agreement of the present fit with data at lower energies is displayed in the comparison with the 5.9 GeV/c data in Fig. 8. (There is, in addition, an apparent systematic discrepancy with the data from Serpukhov.)

The authors have also compared their fits to the charge exchange reaction with the difference in the π^-p and π^+p cross sections. Assuming that the forward charge exchange cross section continues to fall with increasing s in the same manner as observed up to 200 GeV/c, the authors determined the ratio of the real to the imaginary part of the forward amplitude using a dispersion relation. This, along with the recognition that the imaginary part of the forward charge exchange amplitude is related to the difference in the π^-p and π^+p total cross section enabled them to check the consistency of their data with that of reference (2). The successful result of this check (and of dispersion relations, isospin invariance, and the optical theorem) is displayed in Fig. 9.

Just as the pion charge exchange reaction is believed to be dominated through the exchange of the ρ trajectory, the reaction $\pi^-p\to\eta n$ is expected to proceed through A_2 exchange. This reaction has now also been measured at Fermilab [4]. Near 100 GeV/c the η

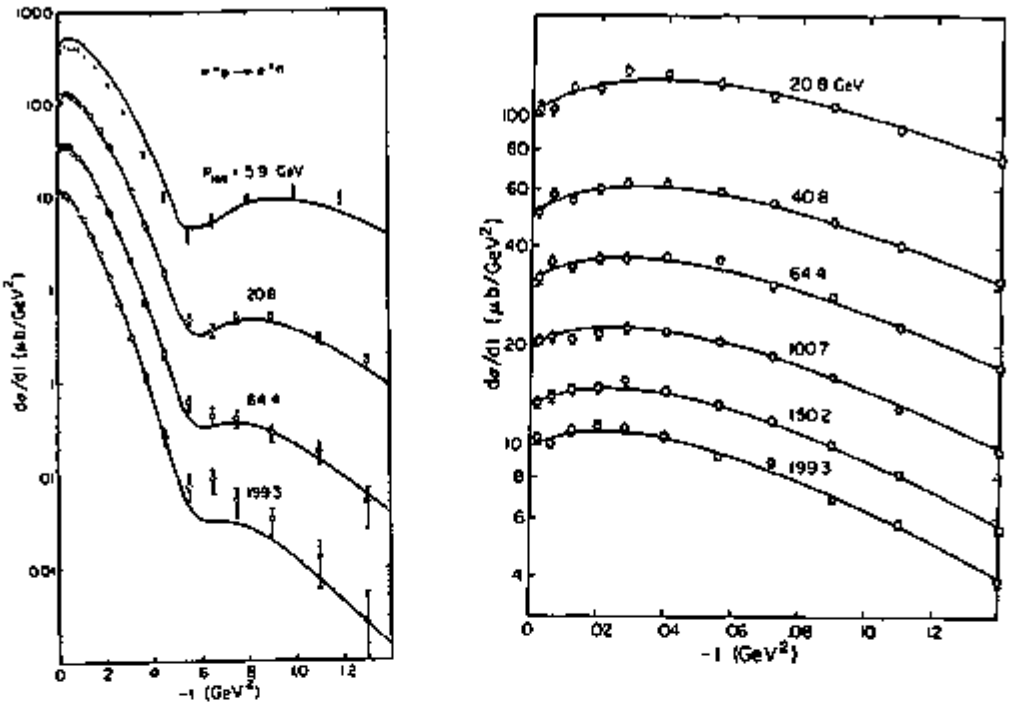

Figure 8: Differential cross sections for $\pi^- p \to \pi^0 n$ between 20.8 GeV/c and 199.3 GeV/c. The data at 5.9 GeV/c are from a previous investigation.

production reaction has a cross section of ∿0.8 μb, compared to the charge exchange cross section of ∿3 μb. The data and the authors' fit to the A_2 trajectory are shown in Fig. 10. The properties of this reaction appear to be quite similar to those noted for the charge exchange process. Again, except in just a qualitative way, the fit to α_{A_2} at high energies is not very consistent with the results at low energy. (In particular, the extracted value of $\alpha_{A_2}(0)=0.37\pm0.01$, is low again.) Because the effective ρ and A_2 trajectories do not have the same slopes or intercepts this obviously means that they are not degenerate for $t<0$. And since there is no established $J^P=4^+$ partner to the A_2, it is not clear what is the situation for $t>0$. In any case, the concept of exchange degeneracy which has often been taken as an article of faith must be considered, at best, a poor approximation to reality.

In contrast to pion charge exchange, neutron-proton charge exchange cross sections exhibit characteristic sharp peaks (with widths of ∿0.02 GeV^2) at t=0. Measurements of differential cross

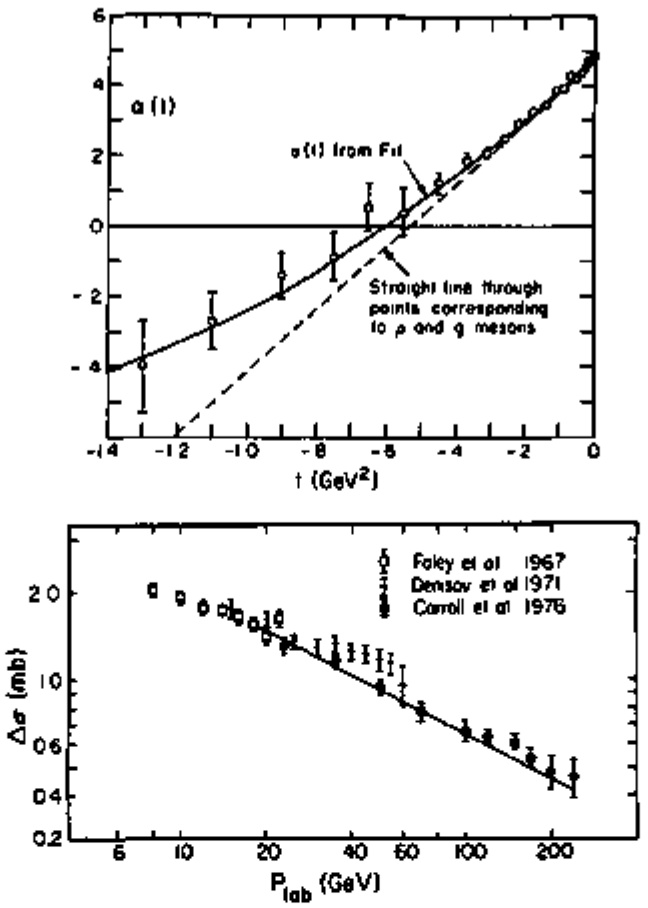

Figure 9: Fit to an effective Regge trajectory $\alpha(t)$ for the reaction $\pi^- p \to \pi^0 n$. The bottom graph provides a comparison of the measured difference in $\pi^- p$ and $\pi^+ p$ total cross sections with the difference expected from an analysis of the charge exchange process.

sections for neutron-proton charge exhange for incident momenta between 60 GeV/c and 300 GeV/c are shown in Fig. 11. [20] The authors remark that, although the absolute cross section falls by a factor of $\sim 10^5$, the shape of their spectra is essentially the same as observed near 1 GeV/c. The total cross section falls as p_{lab}^{-2} between 2 GeV/c and 12 GeV/c, as $p_{lab}^{-1.5}$ near 50 GeV/c and as p_{lab}^{-1} at FNAL energies. The sharp peak near t=0 is reminiscent of reactions which are dominated by pion exchange. The data at low energies do, in fact, agree with the presence of a large non-flip contribution from pion exchange. The onset of a shoulder in the cross section at $t \approx 0.1$ at high energies may be due to the emergence of contributions from higher lying trajectories

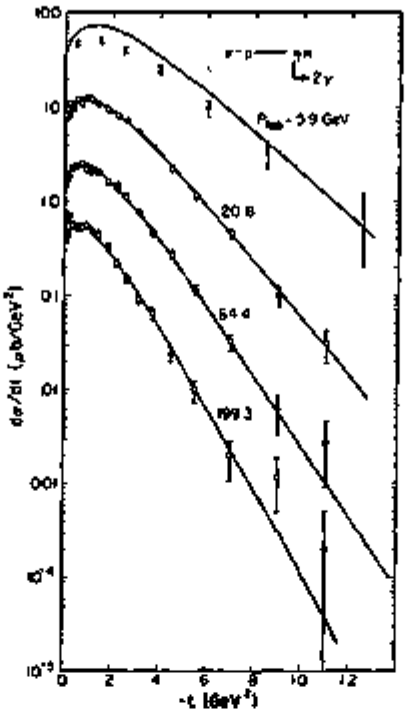

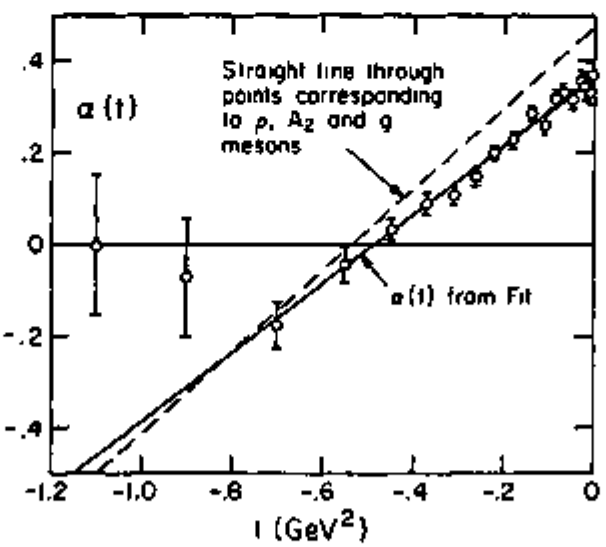

Figure 10: Phenomenological fits to the data for $\pi^- p \to \eta n$. The effective Regge trajectory $\alpha(t)$ should correspond to the A_2 meson.

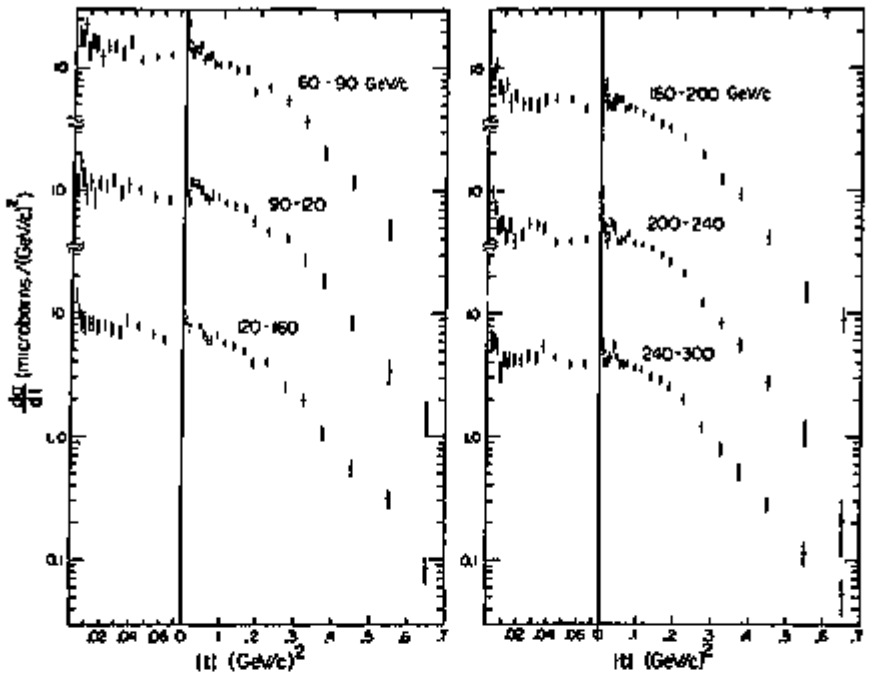

Figure 11: Data for the charge exchange reaction np → pn at Fermilab energies.

which were overwhelmed by the pion term at small s. Figure 12 displays the author's fit to an effective exchange trajectory for the process. Unlike the results at lower energies, the effective $\alpha(t)$ has more resemblance to a vector-meson than to a π trajectory. This is not entirely surprising because the π-exchange contribution falls rapidly with increasing energy. But then arguing this way makes the presence of the steep peak at $|t| \lesssim 0.02$ somewhat enigmatic.

From an extrapolation of the fitted np charge exchange data to t=0, the authors have provided a bound on the absolute difference between the pp and np total cross section as a function of beam momentum. These bounds are far more stringent than those available from direct measurements of the individual total cross sections. At 250 GeV/c, for example, the expected difference can be no greater than 0.30±0.03 mb.

I conclude this section with the note that the simple Regge ideas have fared surprisingly well in their confrontation with the charge-exchange data. Although exchange degeneracy has been dealt a severe blow, the essential features of the Regge-pole

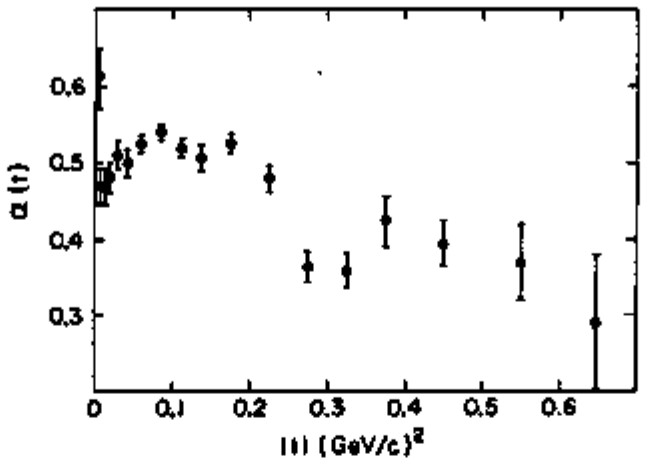

Figure 12: Effective Regge trajectory for the data displayed in Fig. 11.

exchange mechanism have survived the stringent tests of ultra-high energies. The small changes in the effective-trajectory parameters can certainly be attributed to absorption effects or to the presence of contributions from other non-leading exchanges which cannot be ignored at low energies. For the np charge exchange reaction matters are somewhat less clear, but here the low-lying π-trajectory is involved and consequently the test of Regge ideas are more muddled by possible contributions from cuts and strong absorption.

II. INELASTIC DIFFRACTION PRODUCTION

Selected Exclusive Channels

An extensive investigation of the dissociation of neutrons in the reaction $np \to (p\pi^-)p$ is presently in progress [21]. Preliminary results, which have recently been published, [22] indicate that the decay properties of the produced $p\pi^-$ system can be described quite well in terms of a diffractive Deck model involving pion as well as proton exchange graphs. Figure 13 provides the essential features of the data. The $p\pi^-$ mass (M) spectrum has a characteristic accumulation at low mass and shows, in addition, resonance structure near 1500 and 1680 MeV. The t distribution of the $p\pi^-$ system is sharply peaked at small angles, as is the case in all diffractive processes. Although the t spectrum for all M shows substantial curvature near $t \sim 0.1$, it can be approximated rather well by an exponential for $t \lesssim 0.2$ when the data are not integrated over M (i.e., at fixed M). The decay angles of the

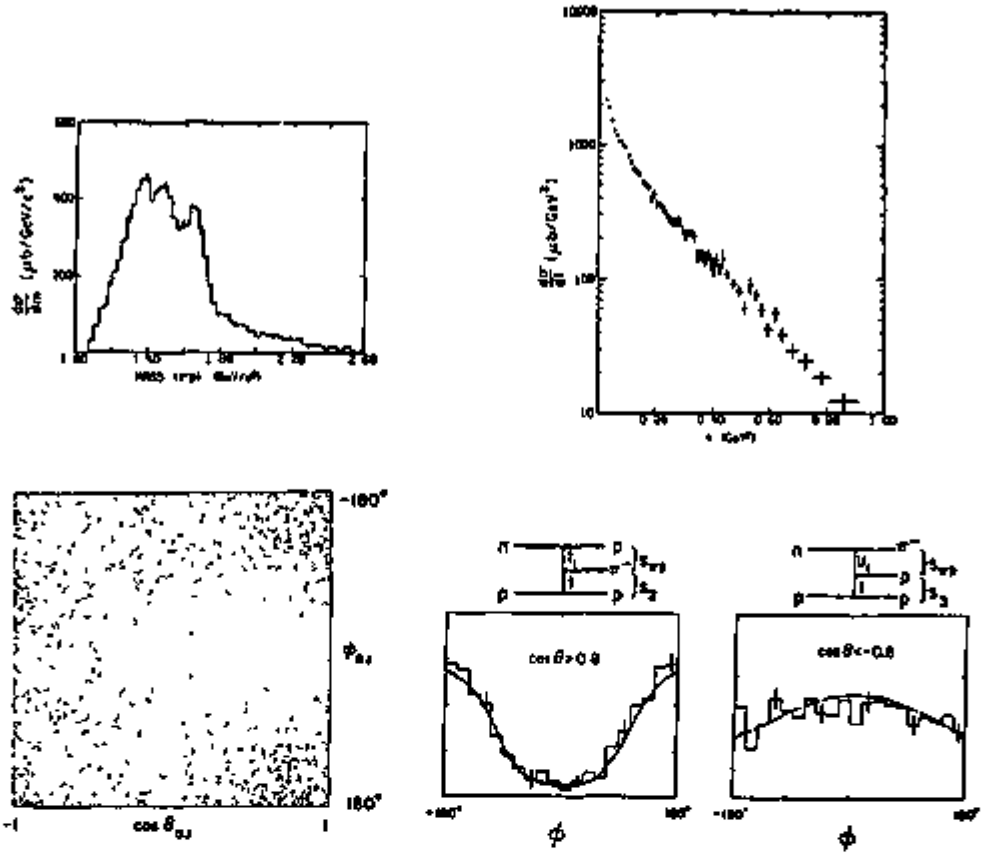

Figure 13: General characteristic of the reaction $np \to p\pi^- p$ at Fermilab energies.

proton as examined in the Gottfried-Jackson frame of the $p\pi^-$ system (for M<1.4 GeV) are also shown in Fig. 13. The scatterplot displays the sort of structure expected from the dominance of Deck processes in the production. The pion-exchange contribution is dominant for $\cos\theta \sim 1$ and the proton exchange near $\cos\theta \sim -1$. (Because there are no known $I=\frac{1}{2}$ baryon resonances below M=1.4 GeV, I would regard with suspicion fits to these data which involve only the super-position of the π-exchange diagram and resonance production.)

Figures 14, 15, 16 and 17 display some other striking and rather unexpected features of these same data. Simple exponential fits have been performed to the t spectra as a function of M. Figure 14 displays the slopes in t obtained in these fits. At the threshold in $p\pi^-$ mass the slope is about two times larger than observed in elastic pp scattering at comparable t-values. This immediately suggests that the diffraction process takes place at

larger impact parameters than elastic scattering. The slope falls almost linearly to a value of 5 GeV^{-2} at M$\sim$1.55 GeV, above which it is constant. An interesting shoulder is observed in the slope at M$\sim$1.35 GeV.[23] There is essentially no energy dependence observed for the dissociation process. In Figure 15 I show the slope in t for M<1.4 GeV as a function of momentum. There is no apparent variation in this parameter, although a change of the order of $\sim$5%, as observed in elastic scattering, clearly cannot be excluded by the data. Another characteristic of diffractive processes is the lack of any substantial s-dependence in the cross section. This feature of the data is shown in Fig. 16, where cross sections for specific mass intervals are given as a function of momentum. The absolute values of these cross sections are typically about a factor of two smaller than observed at $\sim$20 GeV/c.

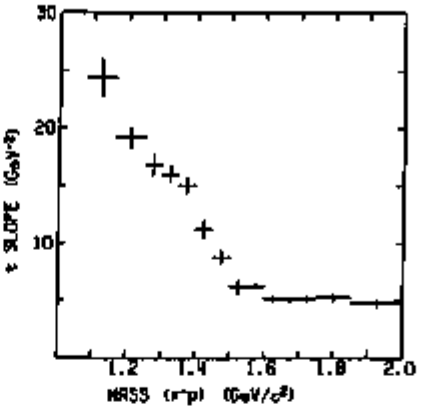

Figure 14: Slope of the t-distribution as a function of the mass of the π^-p system produced in the diffractive reaction $np \to p\pi^-p$.

Last year at my seminar here [22] I showed the t-distribution of the data for two regions of cosθ. E. L. Berger encouraged us to examine the t-dependence on cosθ in more detail and the remarkable result of this effort is shown in Fig. 17 (for M<1.35 GeV). At very forward θ the t spectra display a turn over characteristic of the Deck π-exchange diagram. At large θ the t distribution is rather steep (presumably due to proton exchange). But for $\theta \sim \pi/2$ there is an unusually steep interference dip near t$\sim$0.2 GeV^2 [24]. It is not clear at all what causes this highly peripheral feature of the data. The results for higher mass values are

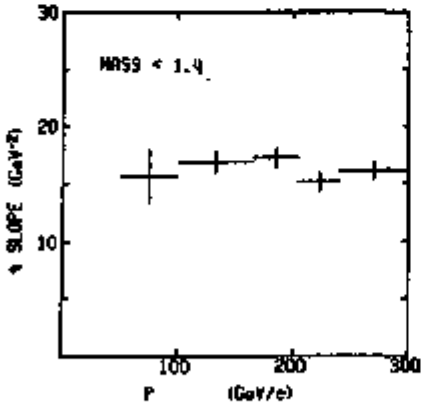

Figure 15: Energy dependence of the t-slope parameter in the reaction $np \to p\pi^-p$.

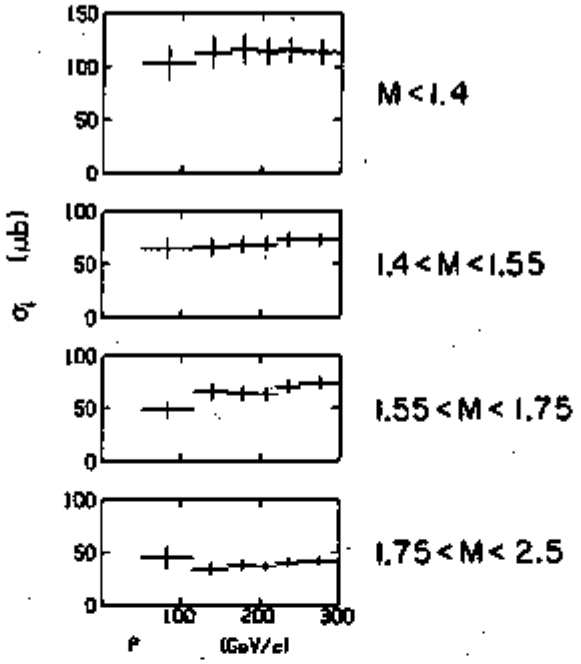

Figure 16: The variation with incident momentum of the cross section for the production of a $p\pi^-$ system of fixed mass M in the reaction $np \to p\pi^- p$.

qualitatively similar, but the sharp dip moves out in t and becomes less pronounced with increasing M (akin to the results in Fig. 14). I would conclude by saying that although the qualitative aspects of these data can be understood on the basis of a Deck model (with absorption), the most striking result, namely the unusual correlation between $\cos\theta$ and t is still to be explained. In addition, it has been emphasized by several authors [25] that when spin is taken into account in the baryon-exchange Deck diagram (spin was ignored in the work of ref. 22), the predicted ϕ distribution for $\cos\theta \simeq -1$ tends to peak at $|\phi| \sim \pi$, which would be in disagreement with the data. Obviously, more work is required here to establish the nature of the exclusive diffraction production mechanism.

The double diffractive dissociation (DD) of the proton in the reaction $pp \to (p\pi^+\pi^-)+(p\pi^+\pi^-)$ has been studied at 200 GeV/c and 300 GeV/c [5]. This reaction has been compared to the single dissociation (SD) of one proton in the reaction $pp \to (p\pi^+\pi^-)+p$ to see whether there is evidence for factorization in these Pomeranchukon-dominated processes. At fixed t and M, Pomeranchuk factorization

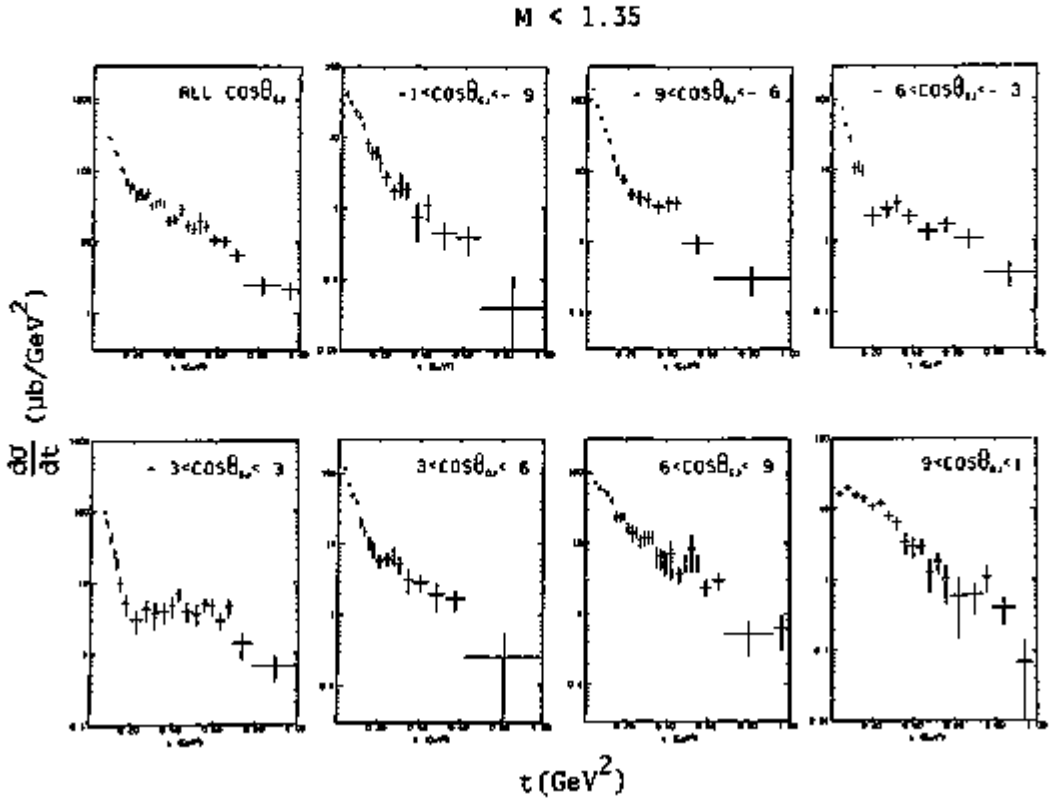

Figure 17: Differential cross sections for the production of a $p\pi^-$ system as a function of the decay angle (θ_{GJ}) of the system in the reaction $np \to p\pi^-p$.

would imply the following relationship between the DD process into masses M_1 and M_2 and the SD processes into M_1 and into M_2:

$$\frac{d\sigma}{dt}(M_1,M_2) = \frac{d\sigma}{dt}(M_1,p)\,\frac{d\sigma}{dt}(M_2,p) \Big/ \frac{d\sigma}{dt}(\text{elastic}).$$

Because of poor statistics the comparison has been performed integrated over M and t. In this case, assuming an exponential t dependence (e^{Bt}) for all the diffractive processes, the relationship for the integrated cross sections becomes:

$$\sigma_{DD} = \frac{\sigma_{SD}^2}{\sigma_{\text{elastic}}}\,\frac{B_{SD}^2}{B_{DD}B_{el}}$$

where also $B_{DD}=2B_{SD}-B_{el}$ must hold to have factorization in t.

Figure 18 shows the actual comparison. The $p\pi^+\pi^-$ mass for the SD data, again, displays the low-mass enhancement characterizing exclusive dissociation phenomena. The $p\pi^+\pi^-$ mass in the DD

events appears to be considerably broader; however, upon subtraction of background expected from choosing wrong $p\pi^+\pi^-$ triplets (estimated from the non-diffractive $p\pi^+\pi^+$ combinations), the shape of the DD mass spectrum becomes reasonably consistent with that observed for the SD data. The value of σ_{DD} is 37±10 μb whereas 23±7 μb is expected on the basis of factorization. Also, the value of B_{DD} (integrated over M), is $2.0\pm0.5\ GeV^{-2}$, whereas $2.5\pm0.6\ GeV^{-2}$ is expected (see the distributions in Fig. 18). Although these results are reasonably consistent with Pomeranchukon factorization and with the presence of double dissociation, an excellent additional test would involve a comparison of the expected slopes only for M<1.5 GeV. Here the value of B_{DD} should be <u>larger</u> than B_{el}! (It is, of course, not clear to what accuracy one should expect factorization to hold because of the presence of non-factorizable absorption effects in the final states. In addition, the strong M-t correlation noted in Fig. 14 raises questions concerning the relevance of results on factorization when data are examined integrated over M.)

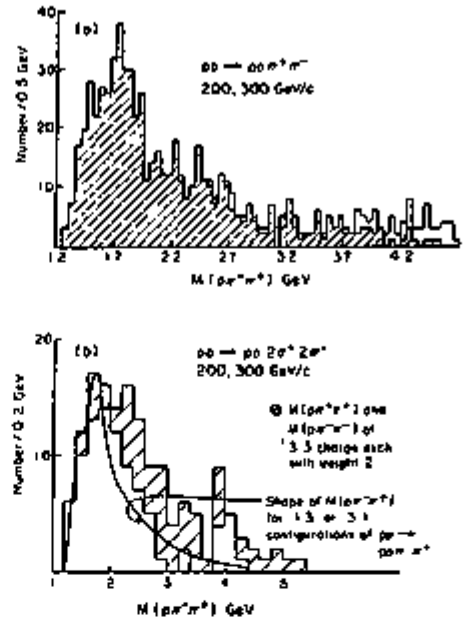

Figure 18: Comparison of single and double dissociation of protons into $p\pi^+\pi^-$ systems.

Inclusive Diffraction Production

As discussed earlier in this lecture, elastic-scattering cross sections are characterized by their very weak energy dependence and their steep angular distributions which peak sharply at t=0. These properties are similar to those expected for the diffractive

scattering of light from an absorbing disk. Certain exclusive channels, such as the above described neutron dissociation into low-mass $p\pi^-$ systems, also exhibit characteristic diffractive properties. In addition to the elastic and to the low-mass dissociation processes which occur at low energies, there exists at higher energies a substantial cross section for the diffractive excitation of a particle into what appears to be a large mass ($M \gtrsim 2$ GeV) continuum. The inclusive channels which are relevant here are those which contain leading particles in the final state, namely, reactions of the kind A+B→A+Anything [26]. When $M^2 \gg 1$ GeV^2 and $M^2/s \ll 1$, a regime which exists only at or above Fermilab energies, the triple-Regge formalism becomes appropriate to this inclusive reaction.

Figure 19 displays the M^2 distribution of the Anything system for the inelastic reactions:

$$\pi^- p \to p + \text{Anything} \qquad (1)$$

$$pp \to p + \text{Anything} \qquad (2)$$

The data are from bubble chamber measurements at 200 GeV/c. [27] The dramatic enhancements at $M^2 \lesssim 25$ GeV^2 in Fig. 19 have two contributions: one is from the dissociation of the projectile particle into low-mass resonances or peaks (such as the 3π A_1 enhancement for reaction (1), and the "N*(1400)" $p\pi$ peak for reaction (2)); the other contribution is from the excitation of the projectile into the multiparticle large-M^2 continuum mentioned above. The total cross section for the peak in reaction (1) is $\sim$2 mb, and in reaction (2) it is $\sim$3 mb (the latter is for the excitation of only one proton). An analogous peak is observed in the reaction $\pi p \to \pi +$Anything, also at the 2 mb level. Hence, the sum of the cross sections for the excitation of either a

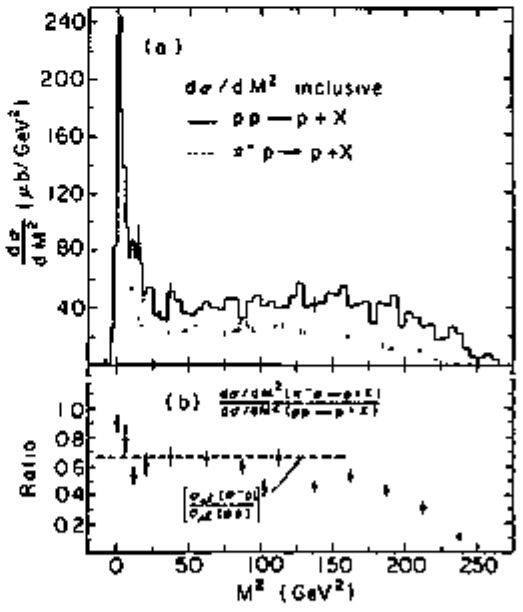

Figure 19: Inclusive cross sections (integrated over t) for the production of protons in the regime of target fragmentation at 200 GeV/c.

target or a beam particle are comparable to elastic scattering cross sections for the same incident channels (3 mb and 7 mb respectively).

Other properties of the peaks at $M^2<25$ GeV^2 can be summarized as follows [26]: (1) The average multiplicity of the events in the enhancement is considerably lower than for events outside of the peak; the multiplicity of the Anything system grows approximately as $\ln M^2$. (2) The cross section for the entire low mass peak is almost energy independent. (3) The t distribution of the M^2 system is sharply peaked at small angles, particularly for the very lowest M^2 (recall the n-dissociation data). (4) These peaks occur only for systems which have the same charge, strangeness, and baryon number as the incident particle. From these characteristics it is reasonable to presume that the low mass enhancement is mainly a diffractive phenomenon involving Pomeranchukon exchange.

Figure 20 illustrates the triple-Regge pole graph which is used to describe the break up of a particle B into a massive system (M). R_i are any Regge poles which can be exchanged. The sum over M is to be interpreted as a sum over all states contributing to the reaction at fixed M^2. The large-M^2 requirement of the model has to do with the substitution of the R_j' Regge pole for the elastic scattering of R on B at $t_j=0$; this is only valid at large M^2, above the resonance region. The triple-Regge formula can be written as

$$E\frac{d\sigma}{d^3p} \approx \frac{s}{\pi}\frac{d\sigma}{dtdM^2} \approx \sum_{ij}\beta_{ij}(t)\left(\frac{s}{M^2}\right)^{2[\alpha_i(t)-\frac{1}{2}\alpha_j(o)]}s^{[\alpha_j(o)-1]}$$

where β is an unknown function of the vertex couplings. When i=j=P (Pomeranchukon), then the invariant cross section at fixed $M^2/s \approx 1-x$ becomes essentially proportional to s/M^2 and s-independent. Also, the cross section $d^2\sigma/dtdM^2$ has a M^{-2} form, independent of energy. When j=V (vector meson) and i=P we obtain another diffractive term which has the approximate form $(s/M^2)^{3/2}\ s^{-\frac{1}{2}}$ for the invariant cross section. At fixed M^2/s this term falls with

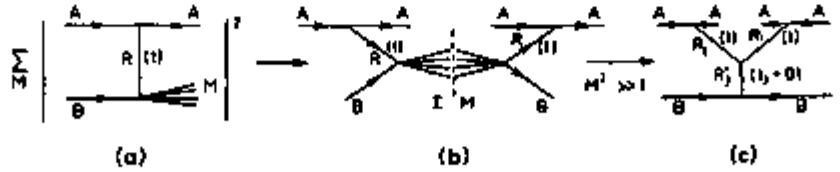

Figure 20: Relationship between an inclusive cross section and the relevant triple-Regge graph.

energy as $s^{-\frac{1}{2}}$. Another interesting situation occurs when i=V and j=P. This non-diffractive R-P-R term scales with energy (i.e., is independent of s) and consequently $d^2\sigma/dtdM^2$ at fixed M^2 falls approximately as s^{-1}. (The above statements are only roughly correct because we have ignored Regge interference [28] terms as well as the t-dependence of the α_j, and have set $\alpha_V(0)=0.5$ and $\alpha_P(0)=1.0$.) The P-P-P term is expected to dominate for small M^2/s. The P-R-P term should also be important at low M^2 and become negligible at very high energy. The R-P-R term should dominate for M^2/s beyond the diffractive peak. Data appear to exhibit the gross features of the triple-Regge parameterization.

Figure 21 displays the M^{-2} fall off (beyond the resonance peak which is observed near $M^2\sim3$) expected from the P-P-P term for the large-mass diffractive excitation of target protons in π^+p and pp reactions between 140 GeV/c and 170 GeV/c [29]. The authors have extracted the P-p total cross section and the P-P-P coupling constant from their $\pi^\pm p$, $K^\pm p$ and $p^\pm p$ proton-fragmentation data. The results from all channels agree; i.e., cross sections factorize to $\sim$10% accuracy and the P-p cross section can be written in the factorized form [29]:

$$\sigma_{tot}^{Pp}(M^2,t) = \left[M^2 \frac{d^2\sigma}{dtdM^2} \Big/ \frac{d\sigma}{dt}_{elastic}\right] \cdot \sqrt{16\pi(d\sigma/dt)_{pp}}$$

the expression in the bracket refers to the ratio of inclusive and elastic scattering for the same incident channel. The value of $\sigma_{Pp}(t)$ is independent of M^2 (Fig. 21) and equals $2.9\exp(-1.04t+0.35t^2)$mb; at t=0 the P-P-P coupling constant r_o is 0.80 ± 0.03 GeV^{-1}. (It is interesting that at larger values of M^2, where the PPP term is no longer expected to dominate, factorization is grossly violated in pp data relative to πp and Kp channels [30]. This can be attributed, for example, to the presence of different RPR terms, such as $\pi P\pi$, in the pp as opposed to the meson-proton reactions.)

The energy dependence of the πp and Kp data at low M^2/s has been checked and appears to exhibit an $s^{-\frac{1}{2}}$ component, particularly at small t, similar to that observed for older pp results [26].

In summary, there exist at high energy large cross sections for the diffractive excitation of hadrons into multiparticle systems. The cross section for the inelastic excitation of a proton in a pp collision is $\sim$3 mb, and that of a pion in a πp collision is $\sim$2 mb. Consequently, the total diffractive, essentially energy independent cross section (elastic, inelastic, and estimated double diffractive) is $\sim0.4\ \sigma_{TOT}$, for both πp and pp data. The inclusive leading-particle distributions in $\pi^\pm p$, $K^\pm p$ and $p^\pm p$

reactions at large x values are consistent to ∿10% accuracy with factorization of the Pomeranchukon contribution to the cross section. The triple Regge formalism appears to yield a surprisingly good description of the data [28].

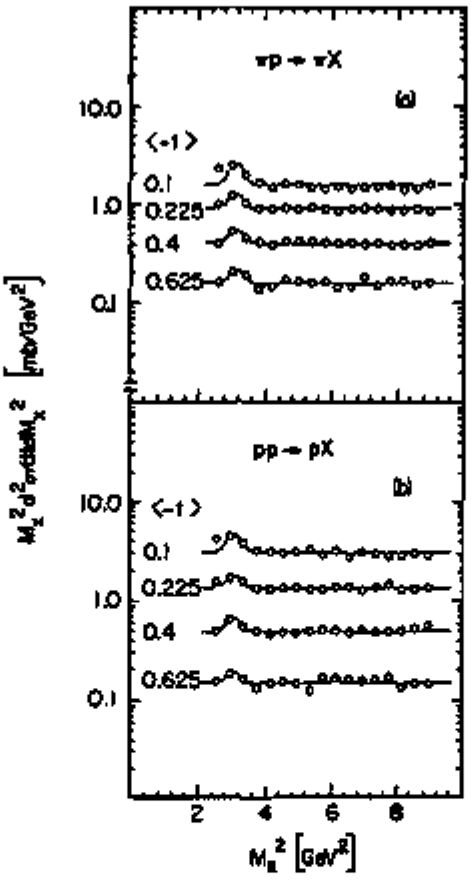

Figure 21: Test for the presence of the triple-Pomeranchukon contribution to leading-particle reactions.

III. INCLUSIVE PARTICLE PRODUCTION

Nuclear Targets

Multiparticle production off nuclear targets can, in principle, be used as a tool for examining the space-time development of hadronic processes. For example, if the asymptotic hadron final state in a hadron-nucleon collision evolves in a distance far shorter than the nuclear dimension, then in a hadron-nucleus collision we might expect that the final-state particles emitted

in the initial interaction of the hadron with a particular nucleon will collide again with the downstream nucleons in that same nucleus, initiating a high-multiplicity cascade. On the other hand, if the initial collision involves the production of a resonant system which decays outside of the nucleus, there would then be very little cascading expected. Consequently, if the hadron-nucleon interaction time is short we expect, naively, that the charged-particle multiplicity in a hadron-nucleus collision will be a strong function of atomic number A and energy. On the contrary, the A dependence and s-dependence should be weak if the time scale for the development of the hadron final state is long.

Figure 22 presents the ratio (R_{NE}) of the inelastic charged-particle multiplicity in nuclear emulsion (average A~73) to that in pp collisions as a function of laboratory momentum [31]. After an initial increase of R_{NE} at energies below 100 GeV/c, the multiplicity in nuclear emulsion is observed to saturate at a value well below R_{NE}=2. This well-known result from cosmic ray studies, supplemented by new data from FNAL, speaks against a cascade model for production in nuclei and for a rather long time-constant for the development of the final state.

Busza et al [31] have performed a series of measurements of multiparticle production in $\pi^{\pm}$, $K^{\pm}$ and $p^{\pm}$ interactions with nuclear

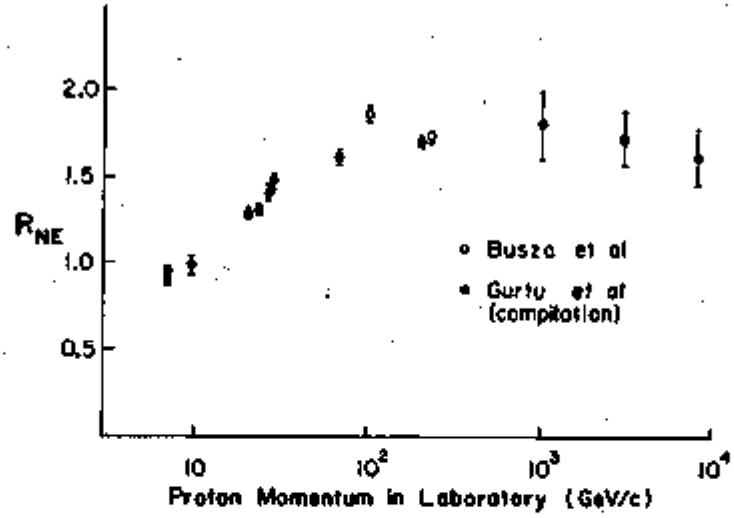

Figure 22: Ratio of inelastic multiplicities for particle production in nuclear emulsion relative to production in hydrogen.

targets ranging from hydrogen to uranium. The data consist of angular distributions of secondaries for 50 GeV/c, 100 GeV/c and 200 GeV/c beam particles. Figure 23 provides a global view of the overall richness of the data. The multiplicity in pA collisions is plotted for different intervals of the pseudo rapidity η, as a function of nuclear target material. ($\eta = \ell n \cot(\theta/2)$, θ is the production angle in the laboratory. η is a good approximation to the laboratory rapidity variable $y = \frac{1}{2} \ell n[(E+p_\ell)/(E-p_\ell)]$, where E and p_ℓ are, respectively, the energy and longitudinal momentum of any particle. η and y become indistinguishable when the transverse momentum is larger than the particle mass, $p_T^2 >> m^2$.) Because of the difference in the inelastic πp, Kp and pp cross sections, and because even large nuclei are partly transparent, the average nuclear thickness of a target material depends on the type of incident particle. A parameter ($\bar{\nu}$) can be defined to take account of this difference in inelastic cross sections for different channels. The value of $\bar{\nu}$ for any nucleus A is given by $A\sigma_{hp}^{inelastic}/\sigma_{hA}^{inelastic}$, where h represents any incident hadron. Thus defined, the $\bar{\nu}$ parameter describes the average thickness of the nucleus in units of absorption mean free paths for hadron h. Also, $\bar{\nu}$ gives a measure of the average number of inelastic collisions h would make with the nucleons if subsequent to each collision it could interact anew.

The data presented in Fig. 23 indicate that the produced multiplicity is strongly dependent on η and on $\bar{\nu}$, except at large η (small angles, or forward production), where the multiplicity is independent of nuclear size. The authors indicate that although pion and proton-induced reactions exhibit different behavior for the same nucleus, the behavior is similar for target nuclei with identical values of $\bar{\nu}$. (The correction for $\bar{\nu}$ is important because, typically, pions have absorption lengths of $\sim$3 f in nuclear matter while protons have absorption length of only $\sim$2f.)

Figure 24 presents a plot of R_A (average multiplicity relative to hydrogen, integrated over η) as a function of $\bar{\nu}$ for $\pi^\pm$ and p data. There is no clear systematic variation of $R_A(\bar{\nu})$ with energy or with the type of incident beam particle. The dependence of R_A on $\bar{\nu}$ requires a quadratic term in $\bar{\nu}$ for an acceptable fit to the data. (For proton data R_A is approximately proportional to $A^{0.25}$.)

In Fig. 25 I show the η spectra for the proton data at 200 GeV/c. As $\bar{\nu}$ (or the nuclear-target size) increases, the multiplicity is observed to grow rapidly everywhere except in the very forward direction.

Although a variety of theoretical models have been suggested in order to explain all these remarkable features of the data [32], the Energy Flux Cascade model [33] appears to be in best overall

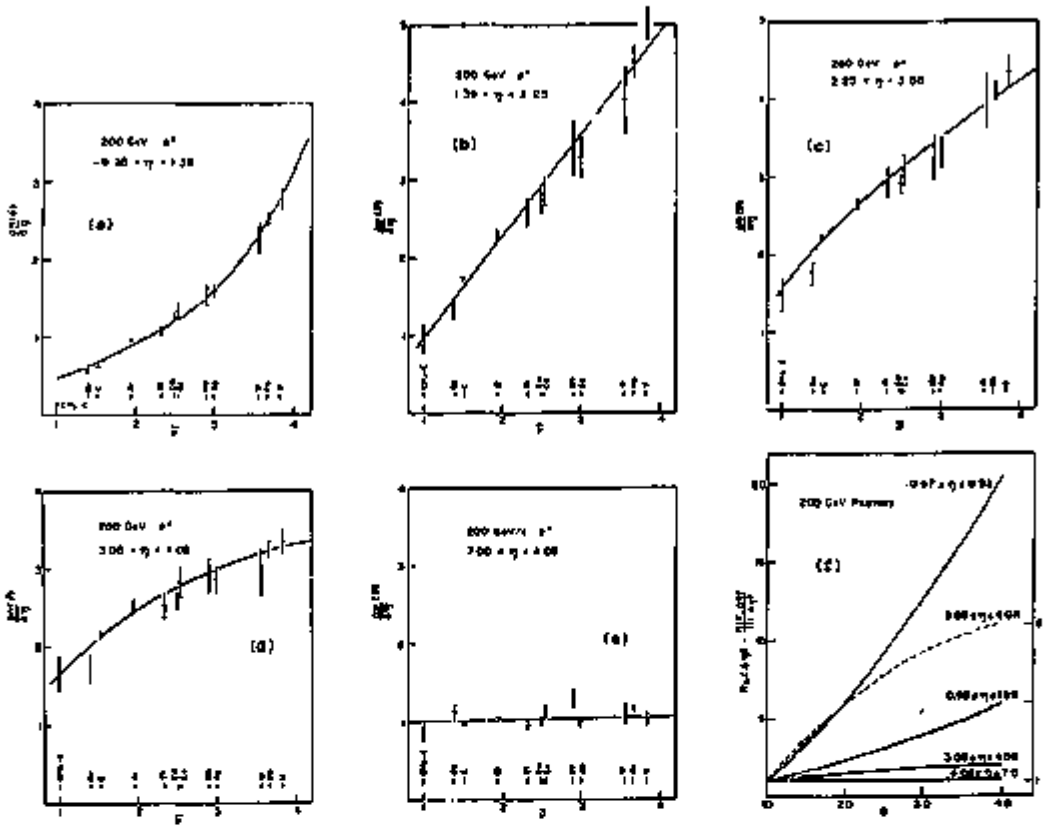

Figure 23: Inelastic multiplicities for particle production in proton-nuclear collisions at 200 GeV/c. The data are displayed for various angular regions (η) as a function of the parameter $\bar{\nu}$ (see text).

agreement with the measurements. In this model it is assumed that the initial collision of a hadron with one of the nucleons in a nucleus generates a distribution of energy which has the same rapidity content as that observed in hadron-nucleon collisions. This energy flux travels through the nucleus, expanding spatially with time, and behaves, as far as its interaction with nucleons in its path, as several systems of hadrons (one large-rapidity pack and perhaps several small-rapidity packs, any group being approximately 1 fermi wide, as measured in the rest frame of that pack). Although all the packs or slices of the original flux can collide with another nucleon, only the large rapidity component has enough energy to produce a new flux (of somewhat lower rapidity content). This process repeats $\bar{\nu}$ times yielding a weak multiplication of particles. Although the Energy Flux Model provides excellent qualitative agreement with the data, quantitative predictions, such as the asymptotic prediction $R_A \approx 1 + (\bar{\nu}-1)/3$, are

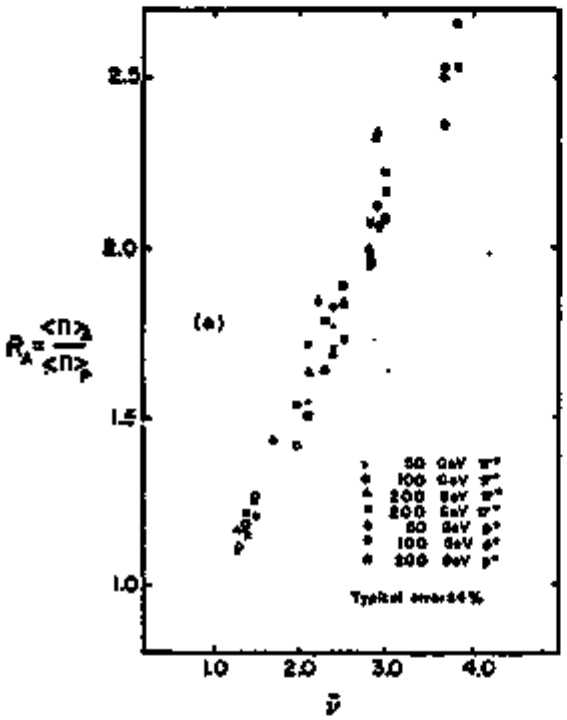

Figure 24: Ratio of inelastic multiplicities for particle production in proton-nuclear and pion-nuclear collisions relative to multiplicities on hydrogen for data between 50 GeV/c and 200 GeV/c, displayed as a function of $\bar{\nu}$.

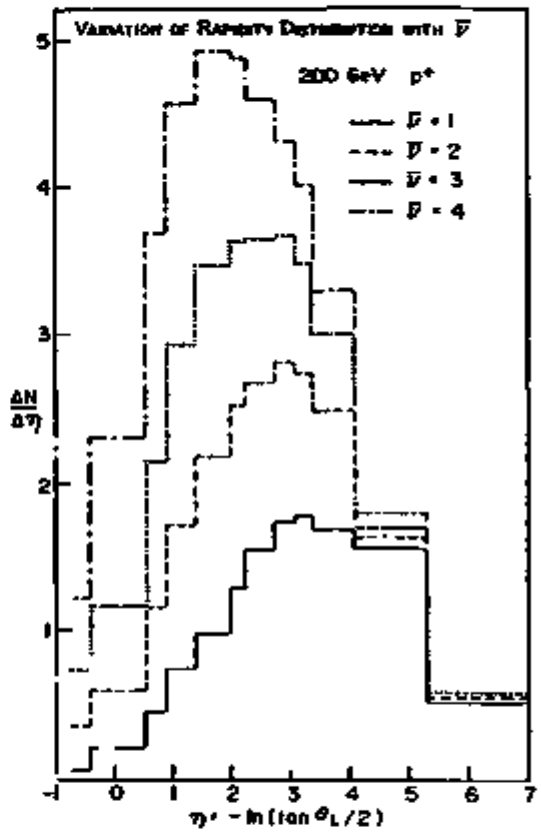

Figure 25: Differential multiplicity distributions as a function of the angular variable η for different target materials for 200 GeV/c incident-momentum protons.

clearly inconsistent with presently available measurements.

The Energy Flux idea certainly appears to come to grips with the problem of multiparticle production in nuclei, nevertheless, there is, perhaps, a more familiar way to understand the above physics. Figure 26 displays the $2\pi^-\pi^+$ and $2\pi^+3\pi^-$ mass distributions observed in inclusive pp collisions at 400 GeV/c. The data indicate that the mean value of the mass spectra are 2-3 Gev, depending somewhat on multiplicity. The widths of these distributions are 1.5-2.5 GeV, comparable to the mean values. Now, if as it is commonly believed, hadron clusters are produced in particle collisions, and the average number of particles in a hadron cluster is ∿3-4 (on the average we have about 4 clusters per pp collision at 400 GeV), we expect that the typical cluster of hadrons produced in high energy collisions will have a mass of ∿2.5 GeV and a width of ∿2 GeV. If the clusters are distributed uniformly in rapidity, then the forward-most cluster will have essentially all the beam momentum and the backward-most cluster will be essentially produced at rest in the laboratory. Because of the localization of the cluster mass, using an uncertainty-principle argument, the fast forward cluster would have an effective lifetime of $\gamma\hbar/\Gamma$ and a mean free path for decay of $\lambda \sim \gamma\hbar c/\Gamma \simeq (400/2)\ (2\times10^{-14})/2 \simeq 20$ fermi! Consequently, if the interaction occurs on a nucleon inside a nucleus, it is clear that the leading cluster will behave as a single massive object as it travels through nuclear matter. Thus time dilation will clearly diminish cascading effects within nuclear matter. If the leading cluster interacts again within the nucleus, the secondary interaction will produce new clusters distributed in rapidity in a manner similar to that in the first collision. Thus the cross section in nuclei at small y will

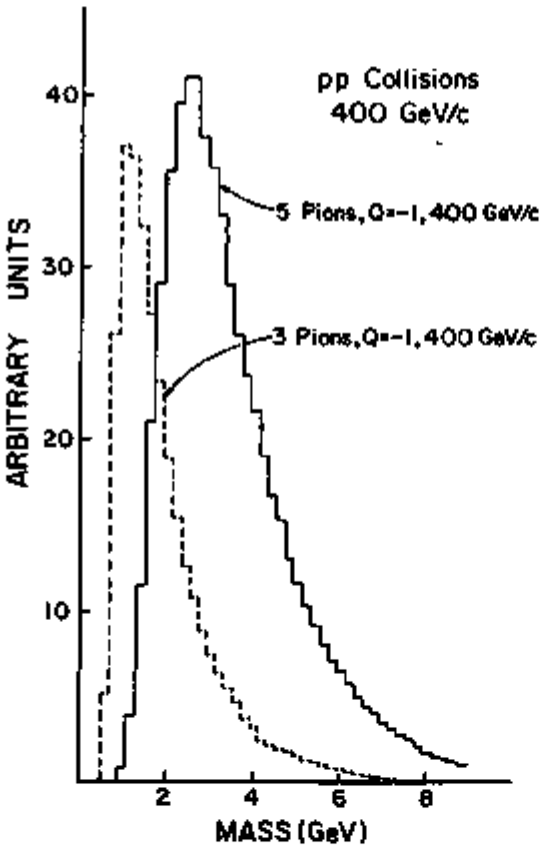

Figure 26: Mass distributions of $2\pi^+3\pi^-$ and $\pi^+2\pi^-$ systems produced in inclusive pp collisions at 400 GeV/c.

be increased as a result of the secondary collisions but the forward y component will not be grossly affected. (The slower secondary clusters will again tend not to have sufficient energy to multiply in the nucleus and therefore the cascading will not be severe.) Although the above remarks are rather qualitative, they may contain the essence of the physics of multiparticle production in nuclear matter [34].

Hydrogen Targets

Multiplicities. One of the general qualities to emerge from investigations of hadron collisions at Fermilab is the essential similarity of all hadronic matter. It appears that the total s-value of a system, and possibly the charge, determine all the major features of multiparticle production in hadronic collisions. Figure 27, taken from reference 5, displays the veracity of these remarks. The figure shows cross sections as a function of charged-particle multiplicities (n) observed in $p^{\pm}p$, $\pi^{\pm}p$ and $K^{+}p$ collisions at 100 GeV/c. Except for the absolute scales, the distributions are all quite similar. In detail, however, differences are apparent between the various channels. In particular, there is an unusually large excess of cross section in $\bar{p}p$ channels relative to pp reactions for $n \gtrsim 12$. The opposite may be true for $n=2$. It will be very interesting to compare $\bar{p}p$ and pp values of σ_n at $\gtrsim$ 300 GeV/c, by which time the cross sections for the $n=4$ multiplicity may also reverse (i.e., $\sigma_{pp}>\sigma_{\bar{p}p}$). I expect this to happen because stronger final-state absorption in $\bar{p}p$ reactions should always tend to reduce $\bar{p}p$ cross sections relative to their analogous pp reactions (such as, for example, the low-multiplicity diffraction channels). In other words, as the $\bar{p}p$ and pp total cross sections become more equal, their small difference will appear, partially at the expense of low-multiplicity reactions, at ever increasing n-values. (I am assuming that the mean multiplicity in the annihilation channel, as in all processes, increases with s.)

Conclusions pertaining to the $\bar{p}p$ - pp difference similar to those reached above have been advanced previously by Eylon and Harari [6]. These authors suggest that on the basis of their model (mentioned earlier in the lecture) the quantity $R_n=[\sigma_n(\bar{p}p)-\sigma_n(pp)]/\sigma_n(pp)$, at fixed s, will approach the form $(3/2)^n$ for large n; also, for fixed n, $-R_n$ will approach the form $(1/2)^n$ at large s. Figure 28 displays a check of the dependence of R_n on n for several s-values [35]. The data have been fitted successfully to the form $R_n=\beta^n s^{-\alpha}$, where the s-dependent parameters β and α appear to approach "asymptotic" values of $\beta=1.24$ and $\alpha=0.73$ at 100 GeV/c. In the specific model of Eylon and Harari β should approach 1.5 while $\alpha/2$ should become equal to the difference between the intercepts of the exchanged meson and baryon trajectories.

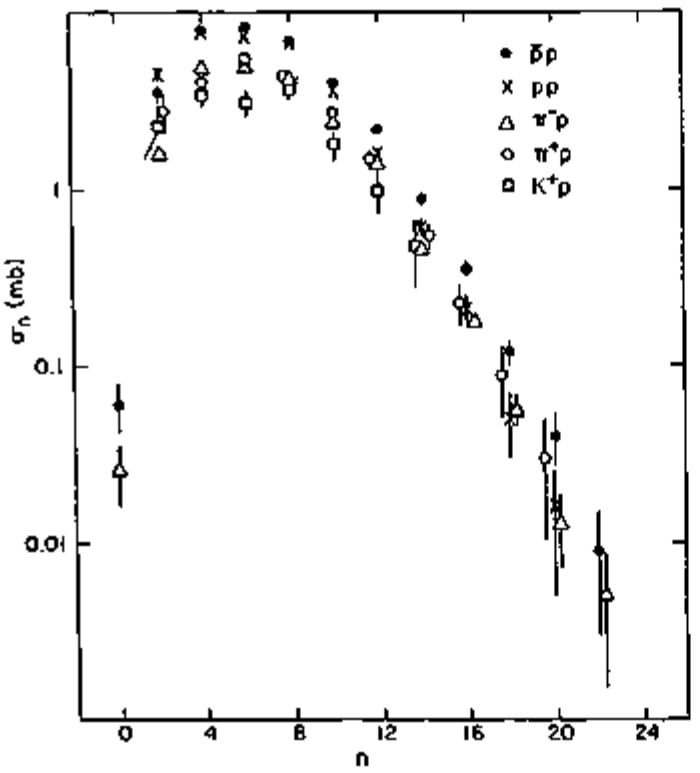

Figure 27: Cross section for producing n charged-particle inelastic final states in hadronic collisions at 100 GeV/c.

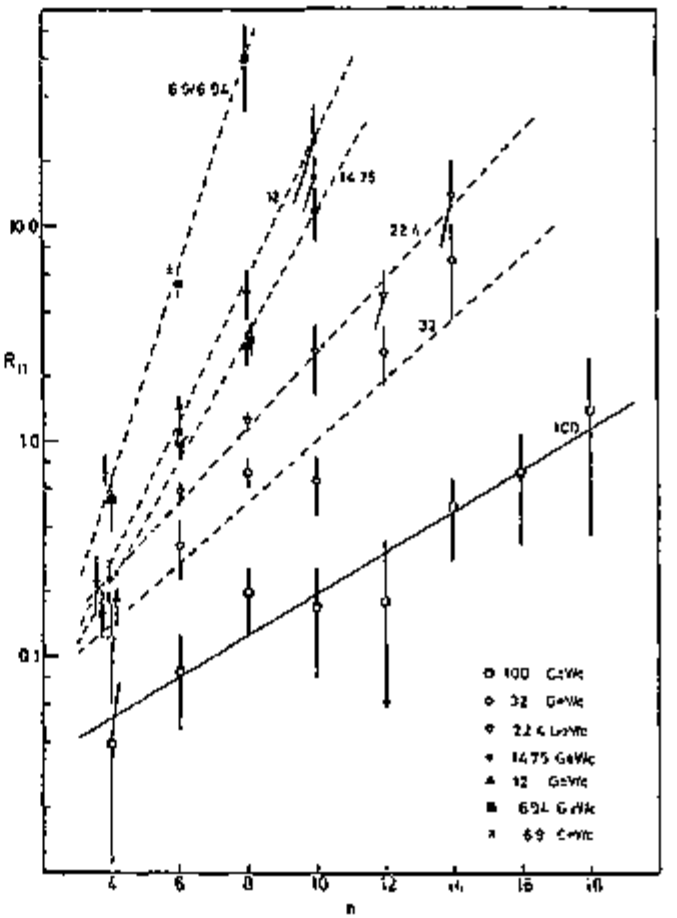

Figure 28: Linear fits to the ratios: $[\sigma_n(\bar{p}p)-\sigma_n(pp)]/[\sigma_n(pp)]$ at different momenta.

Both asymptotic predictions are in rough, albeit surprisingly good, agreement with the data. It is not possible as yet to test whether $-R_n$ approaches $(1/2)^n$. (This is related to the fact that $\Delta\sigma/\sigma(\bar{p}p\to\text{mesons})$ essentially saturates the Eylon-Harari bound of 1, which naively also implies that difference ratio R_n is due entirely to the annihilation contribution to the total cross section.) Nonetheless, as mentioned in the previous paragraph, higher energies may provide a confirmation of the essential prediction that, for fixed n and large s, $\sigma_n(pp) > \sigma_n(\bar{p}p)$.

The dependence of multiplicity distributions on target material is displayed in Figs. 29 and 30. Figure 29(a) compares $\bar{p}p$ with $\bar{p}n$ data at $\sim$15 GeV/c, and Fig. 29(b) compares pp with pn data at 300 GeV/c [36]. (The neutron data were obtained using deuterium targets. The distributions shown in Fig. 29 have been corrected for secondary rescattering and are somewhat model dependent.) Although in detail it appears that the inelastic mean charged-particle multiplicity $\langle n_c\rangle$ tends to be smaller in neutron-target data than in proton-target data, to an excellent approximation, the distributions in Fig. 29 simply interleave as a function of n_c:

$$\sigma_{n_c}(pp) = \tfrac{1}{2}\left[\sigma_{n_c-1}(np) + \sigma_{n_c+1}(np)\right],$$

again suggesting the presence of similar, target-independent, production processes.

Figure 30 displays multiplicity data for π^- on Ne at 200 GeV/c (solid circles), π^- Ne data at 10.5 GeV/c (open squares) and π^-p data at 205 GeV/c (solid triangles)[37]. The multiplicities are presented in terms of the Koba-Nielsen-Olesen (KNO) scaling parameters, [38] where n_π for the Ne data refers to pion shower tracks (i.e., nuclear break-up prongs have been excluded from consideration). Except for the fluctuations in the Ne data, due to enhanced coherent diffraction production at low multiplicities, the three distributions are again very similar, indicating the universality and target independence of multiparticle production processes.

It is well known that the dependence of $\langle n_c\rangle$ on s is not just simply logarithmic [5,26]. Several years ago I showed [39] that the dependence of $\langle n_c\rangle$ on s in pp collisions can be represented using the phenomenological expression $\langle n_c\rangle = A + B\,\ell n\, s + C\,\ell n\, s/s^{\frac{1}{4}}$. The fit was excellent for data from $\lesssim$ 10 GeV/c up to ISR energies. This form is more appealing than an often used quadratic [5] dependence on $\ell n^2 s$ because it provides a way to check whether, asymptotically, multiplicities grow as $\ell n\, s$ and become independent of the incident channel. If all channels yield the same value for the parameter B, the result would suggest (although without a theoretical justification for the above form of $\langle n_c\rangle$) that the

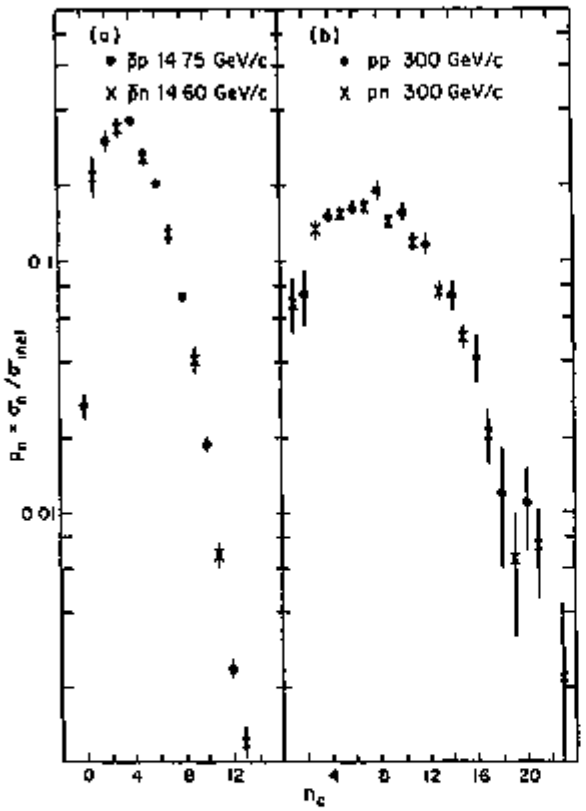

Figure 29: Comparison of $p^{\pm}$-hydrogen and $p^{\pm}$-neutron inelastic multiplicities.

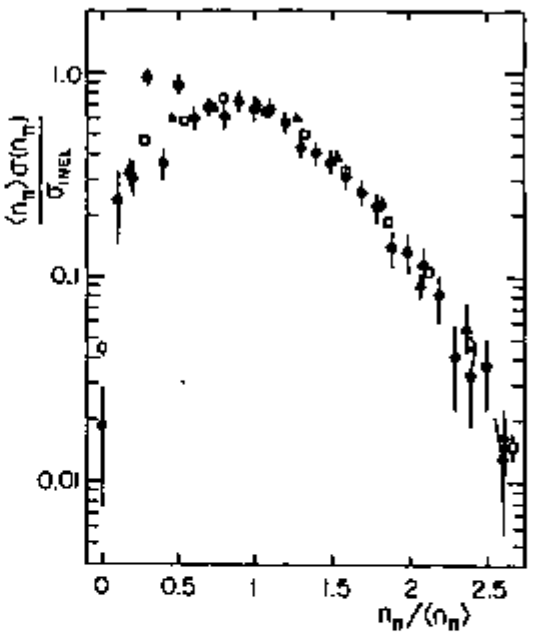

Figure 30: Comparison of π^--Ne data with π^-p multiplicities in terms of the KNO scaling parameters (see text).

small differences which exist in $\langle n_c \rangle$ are only low-energy effects and that at large-s multiplicities grow logarithmically and Pomeranchuk factorization holds. Figure 31 displays the highest energy $\langle n_c \rangle$ data available for γp, $p^{\pm}p$, $\pi^{\pm}p$ and $K^{\pm}p$ [40]. I have tried to restrict the fits to data for $\gtrsim$10 GeV/c incident momenta. Unfortunately, the only available γp measurements are from a low-energy SLAC experiment [41].

The $K^{\pm}p$ and $\pi^{+}p$ data each consist of only three points - just enough to determine the three parameters. The $\bar{p}p$ data have but four points and extend only up to 100 GeV/c. The best measurements are for pp and $\pi^{-}p$ collisions; these extend from $\sim$20 GeV/c to $\sim$400 GeV/c. The results of all the fits are given in Table I, and several of the curves are graphed in Fig. 31. Except for the relatively poor χ^2 for the fit to the sparse $\bar{p}p$ data, the fits and the agreement in the value of B for all the channels is quite impressive! We see that all data are consistent with Pomeranchuk factorization at large s-values to perhaps $\sim$5% accuracy. It would be invaluable to have $K^{\pm}p$ and $\bar{p}p$ data points for momenta in excess of 200 GeV/c (and, of course, any high-energy γp data) to provide a better check of the form for $\langle n_c \rangle$ and of the universality of the B parameter.

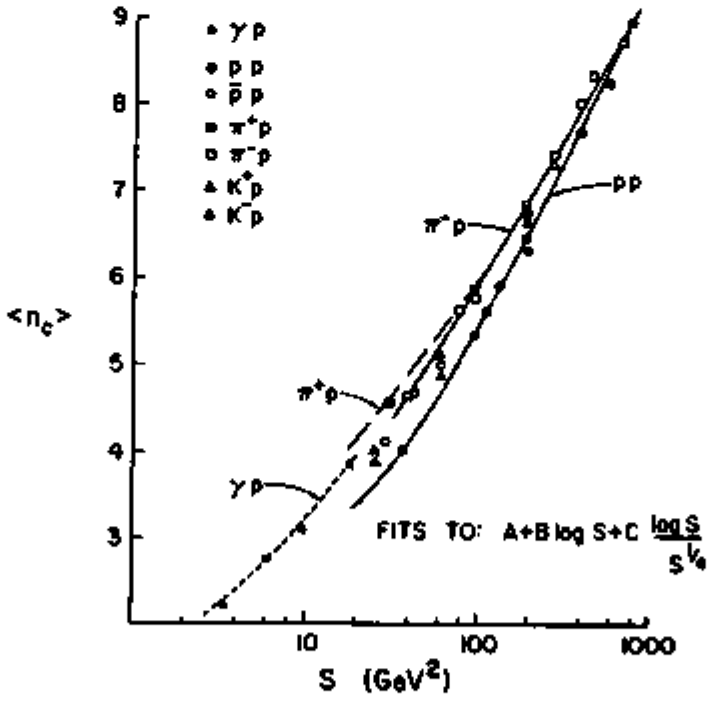

Figure 31: Inelastic average charged-particle multiplicities as a function of s for various hadronic channels. Curves represent fits to the data (see text and Table I).

TABLE I

Fits of Average Charged Particle Multiplicities to the Form:

$$A + B \ln s + \frac{C \ln s}{s^{1/4}}$$

CHANNEL	PARAMETERS A	B	C	χ^2/d.f.
pp	5.35 ± 1.5	1.36 ± 0.05	-4.26 ± 0.92	1.07
$\bar{p}p$	5.44 ± 3.2	1.30 ± 0.07	-3.89 ± 2.0	4.18
K^+p	2.17 ± 5.0	1.29 ± 0.12	-1.57 ± 3.7	-
K^-p	6.38 ± 3.5	1.34 ± 0.10	-4.73 ± 2.3	-
π^+p	3.82 ± 6.3	1.19 ± 0.10	-2.26 ± 4.2	-
π^-p	0.67 ± 1.9	1.40 ± 0.10	-0.82 ± 1.0	1.15
γp	1.67 ± 0.9	1.28 ± 0.53	-1.09 ± 1.6	0.31

Inclusive Production Spectra and Limiting Behavior. Typical rapidity distributions for pions produced in high energy collisions are displayed in Fig. 32 for 102 GeV/c and 400 GeV/c pp data [42]. The data have been integrated over p_T, and no corrections have been applied for ∿10% $K^{\pm}$, ∿1% $e^{\pm}$, and ∿2% $\bar{p}$ contamination. (The estimated corrections required for proton contamination of the π^+ spectra are indicated on the graph.) It is clear from these data that the cross section does not scale in the central region of pion production. In particular, for $y_{CM}=0$ ($y_{LAB}=2.69$ and 3.37 at 102 GeV/c and 400 GeV/c, respectively), the inclusive π^- cross section rises by 45±10%, while the π^+ cross section rises by 30±10% between the two energies. At 400 GeV/c the π^+ cross section is ∿15% greater than the π^- cross section near $y_{CM}=0$, indicating that asymptopia is still far away. For small values of y_{LAB}, where the π^+ yield is about three times the π^- yield, there is some indication that the cross section falls with energy [43]. The π^- data at 102 GeV/c and 400 GeV/c are compared in more detail in Fig. 33. The rise in the invariant cross section with increasing s is clearest at small x. Near $|x|\sim 0.1$ the cross section appears to scale; while at large $|x|$, and especially at small p_T, there is a small violation of the Hypothesis of Limiting Fragmentation [43].

Figure 34 displays invariant cross sections for pion spectra observed in $\pi^{\pm}p$ collisions [44]. The characteristics of these non-leading π-data are similar to those just discussed for pp collisions. Namely, near x=0 the cross section grows with energy,

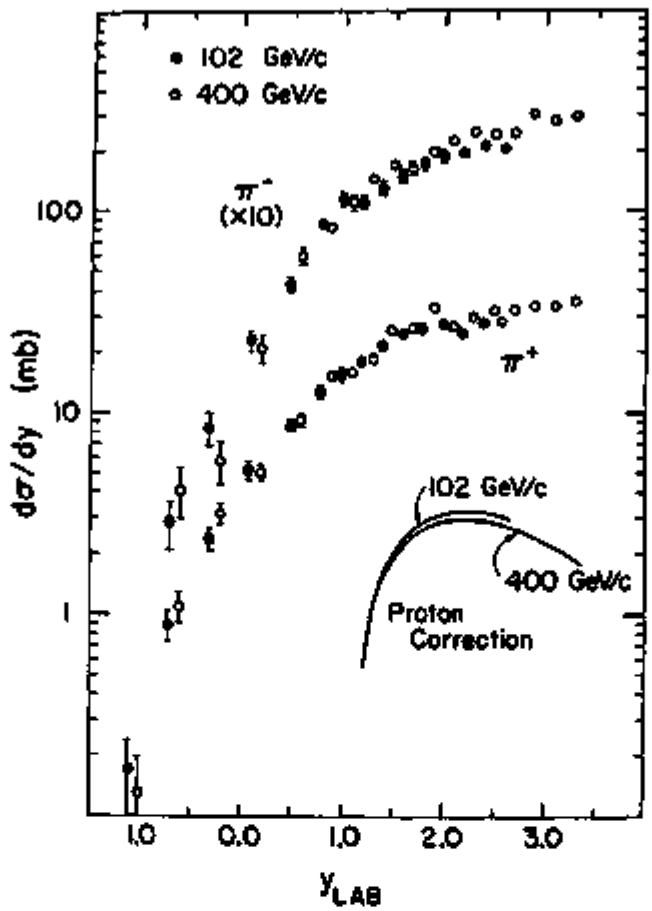

Figure 32: Rapidity distributions (integrated over p_T) of pions produced in pp collisions at 102 GeV/c and 400 GeV/c. Data have not been corrected for $K^{\pm}$, $e^{\pm}$ or $p^{\pm}$ contamination (see text).

while at large $|x|$-values cross sections tend to fall with increasing s.

Whitmore [5] has recently updated and refined an earlier study [45] of the energy dependence of inclusive particle-production cross sections at $y_{CM}=0$. Figure 35, taken from reference [5], summarizes the situation concerning pion production for various reactions. The data are presented as a function of $s^{-\frac{1}{4}}$ in terms of the invariant cross section, integrated over p_T, and normalized by the contributions of the Pomeranchukon to total cross sections for each of the incident channels [46]. (The solid line shown on the graph for π^- production represents recent ISR measurements.)

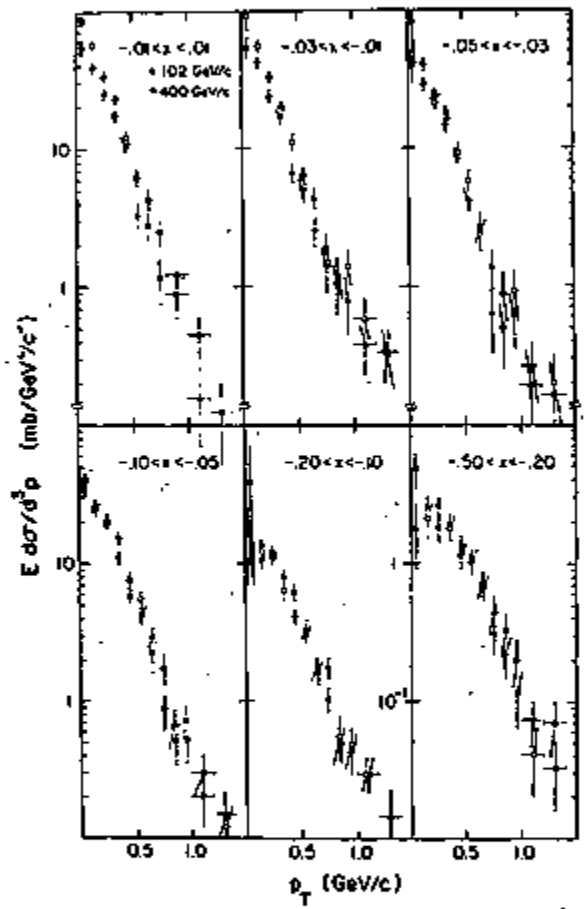

Figure 33: Invariant cross section for negative pions produced in pp collisions at 102 GeV/c and 400 GeV/c, as a function of p_T, for different regions of x. Data have not been corrected for small contamination from e^-, K^- and $\bar{p}$.

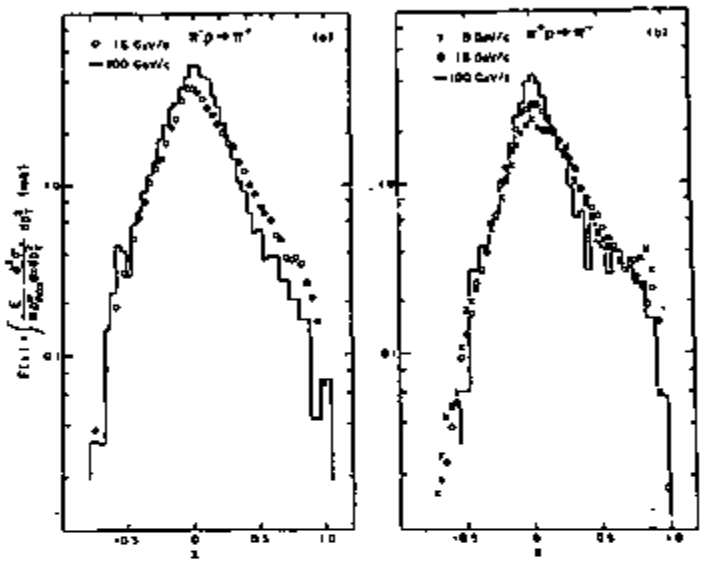

Figure 34: Invariant cross sections, integrated over p_T, for the inclusive production of π^+ and π^- in π^-p and π^+p reactions in figures (a) and (b), respectively.

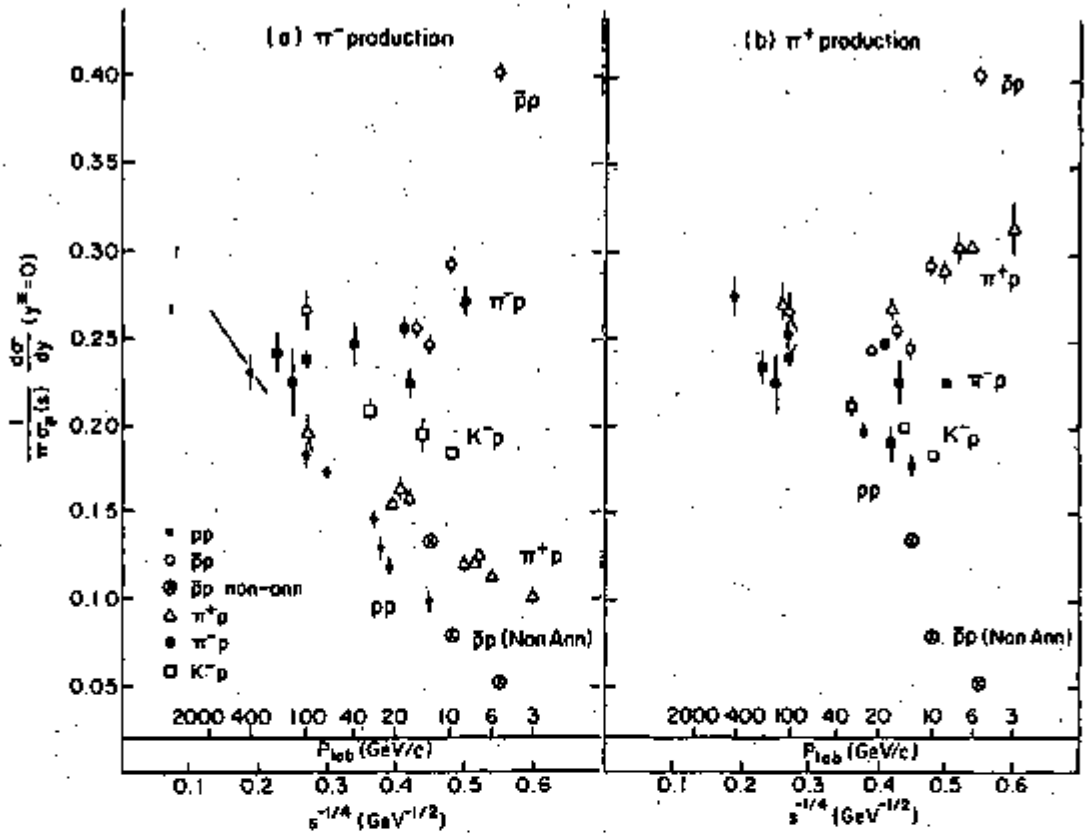

Figure 35: Density function for the production of π^- and π^+ mesons at $y_{CM}=0$, for various incident channels, as a function of $s^{-\frac{1}{4}}$. See text for explanation of the normalization.

Mueller-Regge ideas would suggest that cross sections for π^+ and π^- production should factorize at large s (converge to the same value independent of the incident channel), and, furthermore, the approach to scaling should have an $s^{-\frac{1}{4}}$ dependence. We see that data for all reactions may be converging to the same value of $d\sigma/dy_{CM}$ at $y_{CM}=0$ as $s\to\infty$. As indicated previously [39], this value in Mueller-Regge phenomenology should equal $B/2\pi$, where B is the parameter determining the asymptotic behavior of $\langle n_c \rangle$. From Table I we see that the best value for $B/2\pi$ is 0.21 ± 0.01, a result in rather poor agreement with extrapolations suggested in Fig. 35. I am not certain how to interpret this discrepancy. One possibility, of course, is that the agreement for all B values in Table I is purely accidental. I can, however, take a rather positive view and say that the discrepancy between the extrapolation in Fig. 35 and the value of $B/2\pi$ is only off by $\sim$30% of the extrapolated value! Considering all the theoretical

uncertainties regarding asymptopia, this is, in a sense, still a remarkable result [47].

Independent of the above discrepancy, the data displayed in Fig. 35, and the K_S^0 production data displayed in Fig. 36, suggest that, after leading-particle effects subside, the inclusive cross sections at x=0 increase asymptotically with increasing s, grossly consistent with expectations from Mueller-Regge ideas.

A comprehensive investigation of the approach to limiting behavior of pion production in the target-fragmentation regime has recently been reported in the literature [48]. Figure 37 displays the results of that compilation. The data are presented in terms of an integral of the inclusive cross section over p_T, and over a fixed interval of longitudinal momenta in the laboratory frame (p_L). Specifically, the function $G(p_L)$, which is defined as

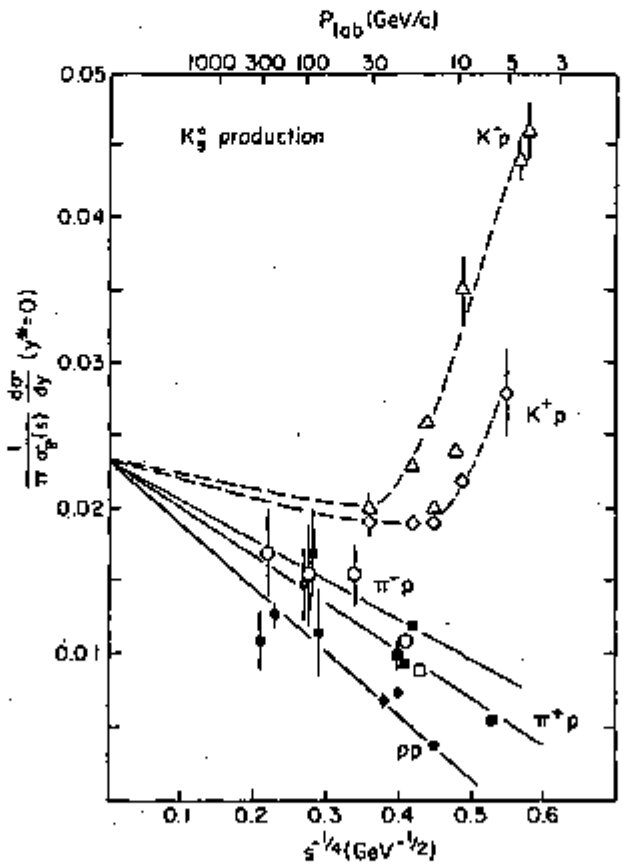

Figure 36: Density function for the production of K_S^0 mesons at $y_{CM}=0$, for various incident channels, as a function of $s^{-\frac{1}{4}}$.

$[\pi/\sigma_p(s)]\int E(d\sigma/d^3p)dp_T^2$, and is normalized as in Fig. 35 by the Pomeranchukon contribution to the total cross section [46], is examined as a function of $s^{-\frac{1}{2}}$. This sort of s-dependence is expected on the basis of application of Mueller-Regge ideas in the target-fragmentation regime for reactions studied in Fig. 37 [49]. Asymptotically all π^- production channels should factorize, and separately, all π^+ production channels should factorize. This appears to be happening at increasing s. At small s-values different channels can have contributions (in addition to the s-independent Pomeranchuk term) from different exchanges; furthermore, if Regge trajectories are not degenerate, and if leading trajectories do not have intercepts of $\alpha(0)=\frac{1}{2}$, then the approach to scaling can be fairly complicated and not just of the $s^{-\frac{1}{2}}$ form. Figure 37 suggests that, in fact, the picture is quite complicated. Nevertheless, the simple exoticity pattern of Chan et al [49] seems to be in qualitative agreement with the data. That is, reactions A+B→C+Anything, where the quantum numbers of (ABC̄) are exotic, display least energy dependence in their inclusive cross sections.

Results similar to those compiled in Fig. 37 have recently been obtained in a counter experiment at BNL and Fermilab [50]. The data are for $K^\pm$, $p^\pm$ and $\pi^\pm$ projectiles incident on protons, in the momentum range between 4 GeV/c and 250 GeV/c. The variation with energy of $\pi^\pm$, $K^\pm$ and $p^\pm$ particle production was examined at a fixed p_T=0.3 GeV/c, and values of y_{LAB}=0.6, 0.4 and 0.2. These global studies indicate that the approach to asymptopia is, again, not just of the $s^{-\frac{1}{2}}$ form. I reproduce one of their graphs in Fig. 38, which summarizes their pion-production results. To achieve factorization of particle-proton and antiparticle-proton inclusive cross sections as $s\to\infty$, the authors require in addition to an energy dependent $s^{-\frac{1}{2}}$ term an s^{-1} term (from lower-lying trajectories) at low energies. Cross sections for meson-proton and baryon-proton channels here again appear to be in agreement with factorization at large s (when using normalizations akin to those suggested in reference [46]).

The SAS Group has also examined inclusive channels involving the exchange of quantum numbers [51]. The available data, which are for the region of projectile fragmentation, have been used to extract the effective Regge trajectories for production at large x values. The specific reactions studied are given in Fig. 39. The authors analyze their data using a semi-empirical one Regge-pole exchange formula, similar to our triple-Regge expression, keeping explicitly the total cross section for the scattering of the exchanged object R(t) on target B (see Fig. 20). The specific form used is:

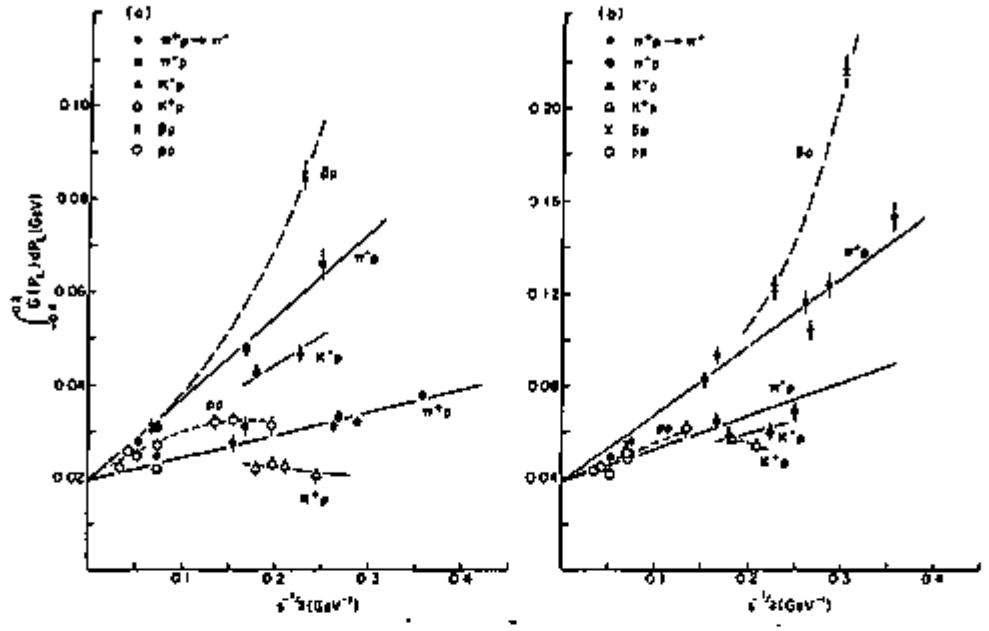

Figure 37: Density function for the production of π^+ and π^- mesons in the region of proton fragmentation in hadron-proton collisions. Data are displayed as a function of $s^{-\frac{1}{2}}$.

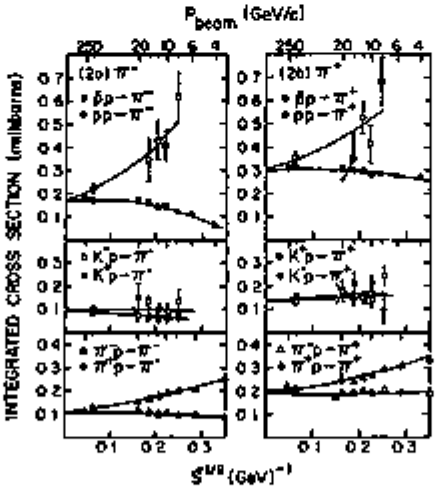

Figure 38: Cross sections for π^+ and π^- production in the region of proton fragmentation for hadron-proton collisions. The integration is over the following final-state momenta and approximate angles in the laboratory frame: $0.3\ \text{GeV/c} \leq |\vec{p}| \leq 0.6\ \text{GeV/c}$ and $50^\circ \lesssim \theta \leq 60^\circ$ (for details see ref. [50]).

$$\frac{d^2\sigma}{dtdx} \approx f(t)(1-x)^{1-2\alpha_{eff}} \sigma_{Rp}(M^2)$$

where f(t) contains all the t-dependence, α_{eff} are the effective values of the exchanged trajectories at the t-values specified in Fig. 39. The energy (i.e.,M^2) dependent cross section for Rp scattering is taken to be the same as for πp, Kp or pp scattering, depending on the nature of the exchanged object (for strange-meson exchange Kp is used, etc.). The data in all but the $\pi^+p\to p+$Anything reaction are consistent with scaling in s to ∿15% accuracy. Consequently, all data in the 50 GeV/c to 175 GeV/c range were combined to study the x-dependence of the cross section. For the $\pi^+p\to p+$Anything process the cross section decreases by ∿30% in the energy range of the experiment, and therefore only 140 GeV/c and 175 GeV/c data were used to extract α_{eff}. The ordinate in Fig. 39 is defined as an average of the cross section over s and t, normalized to the total cross section for Rp scattering at 200 GeV, as follows:

$$\left(\frac{d^2\sigma}{dtdx}\right)_{eff} = \left(\frac{\sigma_{Rp}(p_{in} = 200 \text{ GeV/c})}{\sigma_{Rp}(M^2)} \frac{d^2\sigma}{dtdx}\right)_{average}$$

The values of α_{eff} for exchanges involving K* quantum numbers are $\alpha_{eff}\simeq 0.22$ at $\langle t\rangle_{eff} \simeq -0.3$ GeV^2, amazingly consistent with the K* trajectory. Similarly, the values of α_{eff} for baryon exchange processes typically equal $\alpha_{eff} \approx -0.55$, again in qualitative agreement with expectations from baryon exchange. The difference observed for the cross sections in Fig. 39(a) is presumably due to u-channel nucleon exchanges, which are expected to fall steeply with increasing s (as they, in fact, appear to be doing). The agreement observed between the C-conjugate reactions in Fig. 39(b) is impressive indeed.

Local Compensation of Quantum Numbers. Recent theoretical investigations by Krzywicki and Weingarten [52] have established a new industry for the determination of whether quantum numbers, such as charge, strangeness, baryon number, or even kinematic quantities such as transverse momentum, are locally compensated in rapidity space. The LCQN hypothesis asserts that any produced particle carrying a quantum number q must be accompanied nearby in rapidity space by a small group of particles carrying a total value of the quantum number -q. Local compensation of electric charge had previously been shown to hold [53], and now there is also evidence for the local compensation of transverse momentum in high energy collisions [54].

The best way to illustrate the essence of the LCQN hypothesis is through the idea of a zone graph. Let us consider for simplicity a ten-particle final state produced in a neutron-neutron collision. Two somewhat different possibilities for the distribution of the ten charges in rapidity space are shown in the sketch on the following page. A generalized charge-transfer variable Z(y) can be defined such that for a positive charge located at some particular y, Z(y) increases by one unit at that y value, and for a negative charge, Z(y) decreases by one unit at the position of that charge. The step function Z(y) for a complete event is known as a zone graph. Z=0 separates different zones. In general terms, the LCQM hypothesis requires that for large s-values the internal structure of zones (e.g., mean zone length, number of charges per zone) become s-independent. Furthermore, the properties of zones must be such that it is improbable to have a large number of particles per zone or a zone which is long in rapidity space. Finally, correlations between pairs of zones must decrease quickly with increasing separation in y. Thus stated, LCQM implies that the mean number of zones will grow with energy as $\ln s$. These conditions are fulfilled in a qualitative way for data in the Fermilab energy regime. Figure 40 (from Bromberg et al, ref.[53]), displays the correlation function $D(y_1,y_2)=\langle Z(y_1)Z(y_2)\rangle - \langle Z(y_1)\rangle\langle Z(y_2)\rangle$ for 102 GeV/c and 400 GeV/c pp data as a function of $\Delta y=y_2-y_1$ for $y_1=0$ and $y_1=-1.2$. The curves were obtained by recalculating $D(y_1,y_2)$ after randomly reassigning the charges to

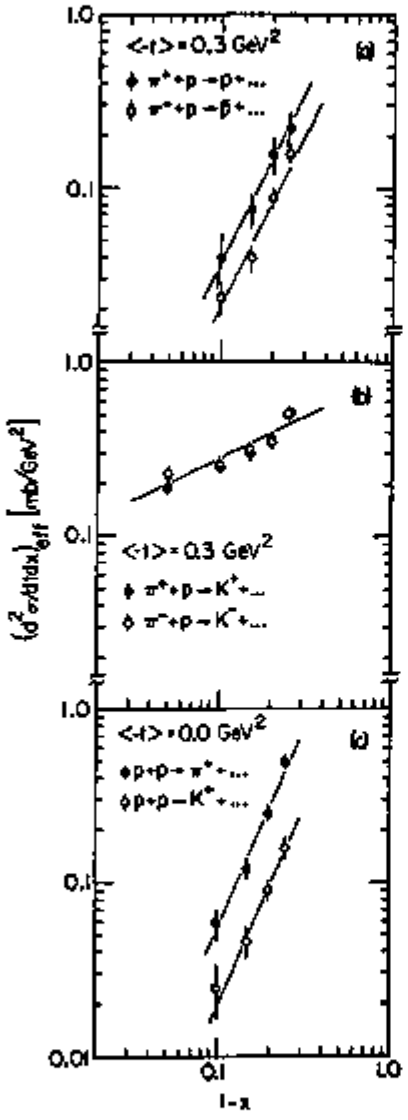

Figure 39: Cross sections for inclusive reactions involving the exchange of quantum numbers.

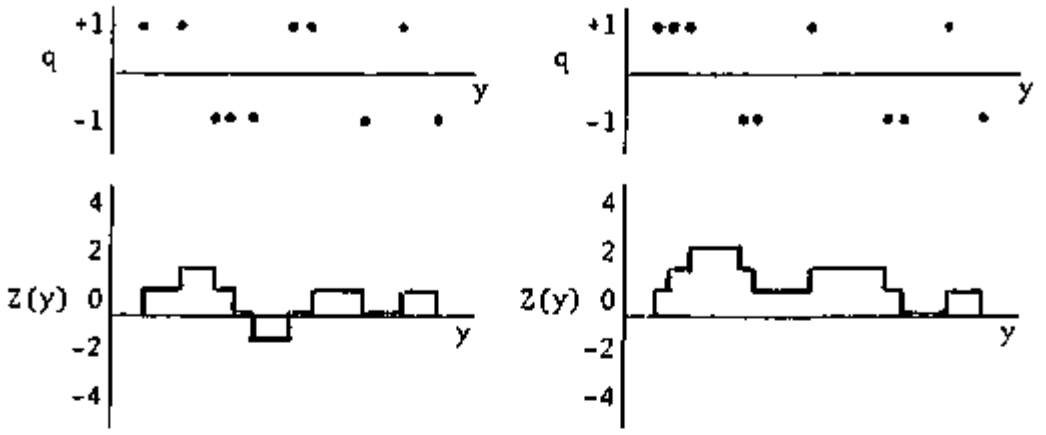

Two Possible Zone Graphs

the observed particle tracks. Hence the difference between the real and the randomized-charges data can be attributed to a mechanism which prevents large fluctuation in charge transfer. In particular, the small value of $D(y_1,y_2)$ reflects a tendency for zone multiplicities to be smaller than for the case of a random distribution of charge, and the rapid fall of $D(y_1, y_2)$ for large Δy, characterized by a correlation length of $\sim$1.2 units in rapidity, shows a tendency for real zones to be typically shorter than in the randomized data, all consistent with expectations from the LCQN hypothesis.

The preliminary results on local compensation of transverse momentum [54] have been used to extract a lower bound on the value of the slope of the Pomeranchukon trajectory. The result is somewhat model dependent in its treatment of unobserved neutrals in the final state, but provides a stringent limit of $\alpha'_P(o) \geq 0.2$ GeV^{-2}, which may be compared with phenomenological values of $\alpha'_P(o) \approx 0.25$ GeV^{-2}. The fascinating implication of this result is that the dynamical mechanism responsible for the shrinkage of the elastic diffraction peak is the local compensation of transverse momentum [54].

Off-Shell Inclusive Scattering. We are all familiar with particle-exchange processes and with inclusive-production reactions. In the past few years interesting data have been presented which indicate that inclusive reactions initiated with off-shell particles bear a great similarity to real inclusive processes.

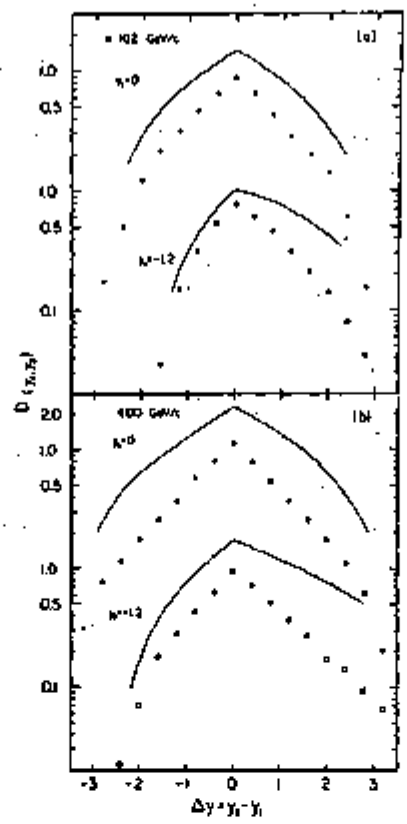

Figure 40: Zone correlation function $D(y_1,y_2)$ for pp data at 102 GeV/c and 400 GeV/c, evaluated at $y_1=0$ and $y_1=-1.2$, as a function of $\Delta y=y_2-y_1$ (y_i are rapidities in the center of mass). Curves are the results of randomizing the charge assignments in each event.

As an example of these sort of studies, I will discuss production of $\Delta^{++}(1236)$ in pp reactions. This process might be expected to proceed through pion exchange, however, this does not appear to be the case. In Fig. 41 I display the π^+p mass distribution for the reaction $pp\to\pi^+p+$Anything at 102 GeV/c and at 400 GeV/c [55]. A clear, energy independent peak at the $\Delta^{++}(1236)$ resonance is apparent in the data. The t-spectrum of the events in the Δ region is shown in Fig. 41(b). In Fig. 41(c) I show the x distribution of the π^+p events in the Δ mass region. The cross section is observed to scale with s. The curve on the data is from a calculation by R. Field. To fit the x spectrum, Field had to introduce a large off-shell damping term (form factor in t) for the pion-exchange contribution to the Δ^{++} process. This form factor was not required for the pion-exchange term in the

pp→p+Anything reaction. In addition to pion exchange, a comparable contribution from ρ and A_2 exchange was required to fit the x distribution. Although it does not appear that pion exchange dominates the production, I will nevertheless compare the characteristics of the X^0 system accompanying the production of Δ^{++} to π^-p scattering at a center of mass energy $\sqrt{s} = M_{X^0}$.

Figure 42 demonstrates that the total charged-particle multiplicity (including "elastic" two-body π^-p final states) of the X^0 system has the same dependence on M^2 as real π^-p data have on s. The f_2 moment ($\langle n^2\rangle-\langle n\rangle^2-\langle n\rangle$) for the X^0 system produced in association with the Δ^{++} also has the same dependence on M^2 as real π^-p data have on s. Taking this comparison one step further, in Fig. 42(c) I display the x distribution for the inclusive reaction $\pi^-p\to\pi^-$+Anything (smooth curve) and the analogous off-shell $R^-p\to\pi^-$+Anything data for several regions of $M^2_{X^0}$. The distributions in Fig. 42(c) have been normalized in such a way that the integral of the data over the invariant phase space yields the values of

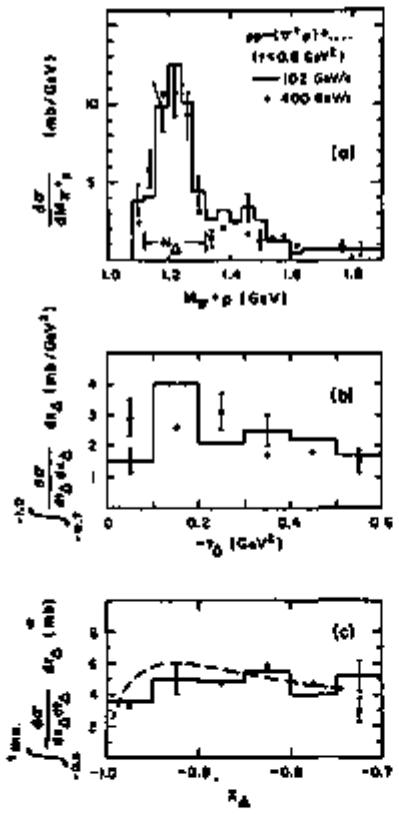

Figure 41: Characteristics of $\Delta^{++}(1236)$ production in pp collisions at 102 GeV/c and 400 GeV/c.

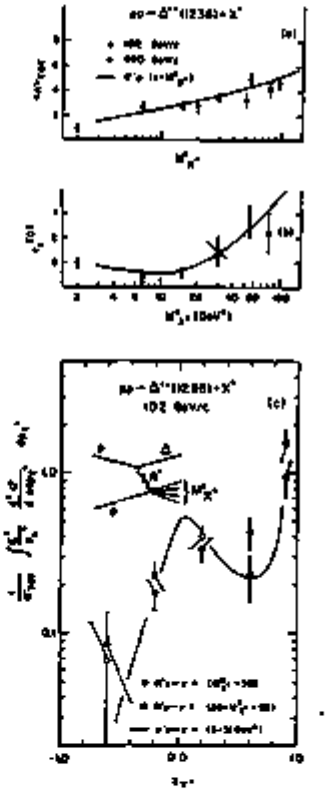

Figure 42: Comparison of off-shell Reggeon-proton (R^--p) scattering with real π^-p production data.

$\langle n \rangle_{TOT}$ given in Fig. 42(a). (The definition of x_{π^-} for R^-p scattering in such that positive x corresponds to π^- emission along the R^- "direction", where the usual Gottfried-Jackson t-channel direction is chosen as the R^-p collision axis.) The similarity between the reaction $\pi^-p \to \pi^- + \text{Anything}$ and the off-shell process $R^-p \to \pi^- + \text{Anything}$ at comparable s values is remarkable. This agreement is particularly puzzling considering the fits that Field made to the Δ production reaction. It appears therefore that the mass and charge of a hadronic system have the greatest bearing on the dynamics. The fact that R^- has admixtures of objects having different spin (but same isotopic spin) does not grossly affect the inclusive spectra.

A similar study to that discussed in Figs. 41 and 42 was also performed for the reaction $pp \to p + \text{Anything}$ [56]. Here off-shell $R^0p \to \pi^- + \text{Anything}$ was compared to $\gamma p \to \pi^- + \text{Anything}$ at values of $s_{\gamma p} \approx M^2$. The inclusive spectra are shown in Fig. 43. The agreement is, again, impressive but quite surprising in view of the fact that for low values of M^2 the R object should mainly have properties characterizing the Pomeranchuk trajectory and certainly not a photon. Consequently, here again we see that gross features of inclusive production appear to be independent of all dynamic qualities, except for the charge and effective mass of the interacting system.

"If there is a question of importance, look to the masses" (Mao Tse Tung). This last part of my lecture can be summarized by the above quotation from Mao's Little Red Book, as paraphrased to me by Ed Berger. We have made a study of the p_T-dependence and the x-dependence of multiparticle systems produced in pp collisions [57]. Specifically, we have examined how the mean value, $\langle p_T \rangle$, and the full width at half maximum of the x distribution (Γ_x) vary with the mass, charge, and particle multiplicity of a produced system. The results of this investigation are summarized in Figs. 44 through 47. There is essentially no dependence on the charge of the system being examined (particularly for $\langle p_T \rangle$). At fixed mass, a weak variation with multiplicity can be discerned in the $\langle p_T \rangle$ data. A somewhat stronger variation is observed for Γ_x. The $\langle p_T \rangle$ dependence is essentially s-independent (between 102 GeV/c and 400 GeV/c) while the Γ_x values become smaller with increasing s (presumably due to approximate Feynman scaling). The variation of Γ_x and $\langle p_T \rangle$ with mass is very similar to that observed for stable hadrons (e.g., π,K,A etc.). In detail, the 3π systems appear to coincide in character with the properties of the long-lived objects [58]. The latter result may be due to the fact that clusters, which have typical multiplicities of $\sim$3, have production properties akin to the more stable particles. (This is not an entirely consistent picture because of the charge-independence of

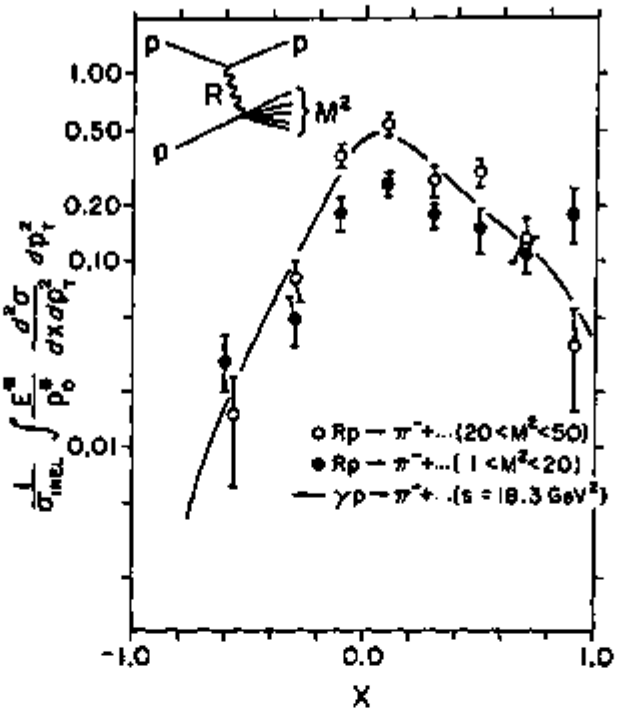

Figure 43: Comparison of the off-shell reaction $R^{o}+p\rightarrow\pi^{-}+$Anything with the inclusive data for $\gamma+p\rightarrow\pi^{-}+$Anything at $s\simeq M^{2}$.

the result.) The rise in $\langle p_T \rangle$ with multiplicity at large masses can be understood, qualitatively, as due to a damped random-walk process. The unusual reversal at small masses may be due to a Bose effect (but here again there is inconsistency because of the lack of dependence of $\langle p_T \rangle$ on charge). The arrows labeled M.C. are the expected values of $\langle p_T \rangle$ (essentially independent of M) which our Monte Carlo model provides for the 400 GeV/c data. (This model contains proper single-particle distributions and multiplicities observed at 400 GeV/c but no explicit correlations among particles.) It is interesting that although the Monte Carlo predictions for $\langle p_T \rangle$ are completely incorrect, the predictions for F_x (not shown) appear to be in far better accord with the data. It is not clear to me whether this new result is important or whether it is just another way to study particle correlations. In any event, the mass of the produced system clearly has the largest effect on the dynamic properties of the hadron bundle, hence one should "look to the masses."

I thank J. Whitmore for providing me with an early version of his update of "Multiparticle Studies Utilizing Fermilab Bubble Chambers". In addition, I wish to thank E. L. Berger, D. Duke,

P. Slattery, and C. Quigg for helpful discussions. Several of the topics in these lectures could not have been prepared without the excellent assistance I have received from our students J. Biel and P. Stix. Finally, I wish to express my gratitude to D. Weingarten for a critical reading of the manuscript and for providing extensive suggestions as to content.

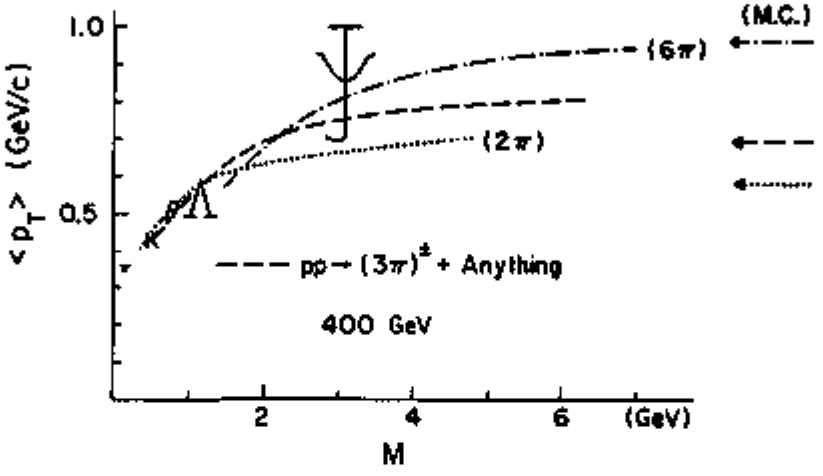

Figure 44: Comparison of $\langle p_T \rangle$ for the production of long-lived particles in pp collisions with 400 GeV/c data (smoothed curves) for the reactions $pp \rightarrow (2\pi)^0$+Anything, $pp \rightarrow (3\pi)^{\pm}$ + Anything, and $pp \rightarrow (6\pi)^0$+Anything. The values of $\langle p_T \rangle$ for the produced multipion systems are displayed as a function of the masses of the systems. (Only charged particles were used for the calculations.)

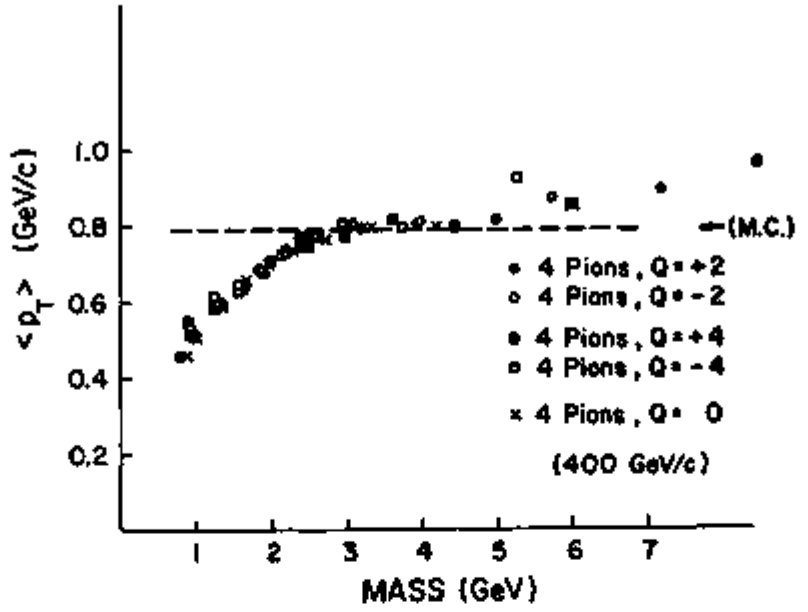

Figure 45: The value of $\langle p_T \rangle$ for a (4π) system produced in the reaction $pp \rightarrow (4\pi) + \text{Anything}$ at 400 GeV/c. This figure displays the variation of $\langle p_T \rangle$ with the mass and the charge (Q) of the (4π) system. The dashed line represents the variation of $\langle p_T \rangle$ with mass, expected on the basis of a Monte-Carlo calculation. (There is only a very weak dependence on charge in the Monte Carlo.)

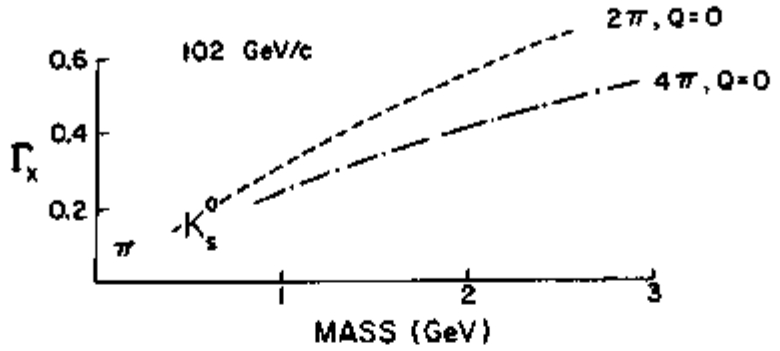

Figure 46: Comparison of the full width at half maximum (Γ_x) of the x-distribution ($d\sigma/dx$, integrated over p_T) for pions and K_s^0 produced in pp collisions at 102 GeV/c with data (smoothed) for the reactions $pp \to (2\pi)^0 + Anything$ and $pp \to (4\pi)^0 + Anything$, also at 102 GeV/c. The widths of the x-spectra are plotted as a function of the masses of the produced multipion systems.

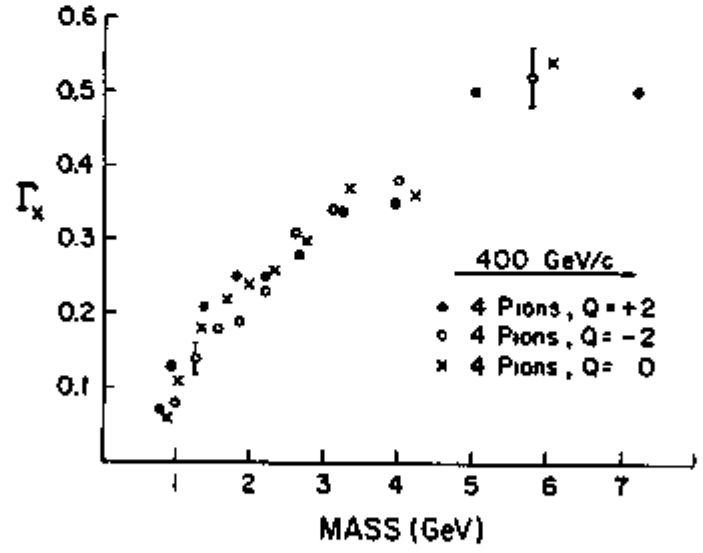

Figure 47: The dependence of Γ_x on the charge of a produced (4π) system in pp collisions at 400 GeV/c.

REFERENCES

1. J.J. Aubert et al, Phys. Rev. Lett. 33, 1404 (1974); J.E. Augustin et al, Phys. Rev. Lett. 33, 1406 (1974).

2. A. Carrol et al, Phys. Lett. 61B, 303 (1976). Also, private communication from W. Baker of the BNL-FNAL-Rockefeller Collaboration.

3. Private communication from H. Kobrak of the Chicago-San Diego-Wisconsin Collaboration.

4. A.V. Barnes et al, Phys. Rev. Letts. 37, 76 (1976). See also O.I. Dahl et al, Phys. Rev. Letts. 37, 80 (1976) for a study of $\pi^- p \to \eta n$.

5. J. Whitmore in Particles and Fields APS/DPF Meeting in Seattle (1975). H. Lubatti and P. Mockett eds. See also the comprehensive review of bubble chamber data by J. Whitmore, MSU Report (Feb. 1976) to appear in Physics Reports.

6. Y. Eylon and H. Harari, Nuclear Phys. B80, 349 (1974).

7. D. Ayres et al (FSAS Group), Phys. Rev. Lett. 35, 1195 (1975); see also the report of D. Cutts which appears in these proceedings. I have included the results of the Michigan-ANL-FNAL-Indiana Group in Fig. 5; see C. Akerlof et al, Phys. Rev. Lett. 35, 1406 (1975).

8. I. Ambats et al, Phys. Rev. D9, 1179 (1974); G. Brandenburg et al, Phys. Lett. 58B, 367 (1975).

9. R.L. Anderson et al (FSAS Group) Fermilab Report Pub-76/47-EXP/ANL-HEP-PR-76-28.

10. M. Davies and H. Harari, Phys. Lett. 35B, 239 (1971). See also R. Carnegie, Phys. Lett. 58B, 371 (1975).

11. Private communication from J. Butler (FSAS Group). See also results of Akerlof et al given in ref. (7). The latter measurements indicate that the ratios $\sigma_{elastic}$ to σ_{total} are 0.15/0.14/0.20 for $\pi^{\pm}p/K^{\pm}p/p^{\pm}p$ channels respectively. The small systematic discrepancies between the two sets of data have been commented on previously by J. Lach, Fermilab Report Conf -76/15-EXP (1976).

12. V. Barger and R. Phillips, Phys. Lett. 60B, 358 (1976).

13. A. Buras and J. Dias de Deus, Nucl. Phys. B71, 481 (1974).

14. See reference 13 for a comparison of pp data, and J. Butler, Ph.D. Thesis, MIT (1975) for a comparison of K^+p data.

15. C. Akerlof et al, Phys. Lett. 59B, 197 (1975). For the initial prediction of Chou and Yang see Phys. Rev. Letts. 20, 1213 (1968).

16. C. Ankenbrandt et al, FNAL-Yale Group, Fermilab-Conf-75/61-EXP (1975). See also J. Lach in reference (11).

17. R. Hendrick and B. Lautrup, Phys. Rev. D11, 529 (1975).

18. V. Bartenev et al, Phys. Rev. Lett. 31, 1367 (1973).

19. V.N. Bolotov et al, Nucl. Phys. B73, 365 (1974). See the lectures of E. Leader for a comprehensive discussion of charge-exchange data and their phenomenological implications.

20. H.R. Barton et al, OSU-MSU-Carleton-Alberta Collaboration, Preprint COO-1545-196. I thank N.W. Reay for a discussion of the data.

21. J. Biel, Ph.D. Thesis, University of Rochester (1976).

22. J. Biel, et al, Phys. Rev. Letters 36, 507 (1976); T. Ferbel, Proc. of Int'l School of Subnuclear Physics at Erice (1975), A. Zichichi ed.

23. This has been emphasized by V. Chaloupka in a preprint discussing similar data from SLAC.

24. A similar effect has been reported by a group at the ISR measuring the reaction $pp \to n\pi^+p$. See H. de Kerret et al CERN preprint (1976).

25. A. Minaka et al, Preprint KYUSHU-76-HE-6 (1976). Also, private communication from E. Berger.

26. For a review of the phenomenology and earlier data see H. Bøggild and T. Ferbel, Ann. Rev. Nuc. Sci 24, 451 (1974).

27. F. Winkelmann, Phys. Lett. 48B, 273 (1974).

28. R. Field and G. Fox, Nucl. Phys. B80, 367 (1974).

29. R.L. Anderson et al, FSAS Preprint (1976). I thank D. Ritson for providing me with this paper prior to general circulation.

30. M. Sogard, private communication from the FSAS Group. See also the paper of D. Cutts in these proceedings.

31. The data are from A. Gurtu et al, Proc. of Vth Int'l. Symp. on Many-Particle Hadrodynamics, Eisenach-Leipzig (1974), G. Ranft and J. Ranft, eds. and W. Busza et al, MIT/Carleton/FNAL preprint (1976). See also W. Busza, VIth Int'l Conf. on Nuclear and Particle Physics, Los Alamos (1975). I wish to thank J. Elias for a helpful discussion of the Fermilab data.

32. See the review of L. Bertocchi, VIth Int'l Conf. on Nuclear and Particle Physics, Los Alamos (1975).

33. K. Gottfried, Phys. Rev. Letters 32, 957 (1974).

34. For an alternate description of multiparticle production on nuclear targets see the report of G. Berlad in these proceedings.

35. R.E. Ansorge et al, Phys. Letts. 59B, 299 (1975); J.G. Rushbrooke et al, Phys. Letts. 59B, 303 (1975).

36. The figure is from reference (5). The pn data are from A. Sheng et al, Phys. Rev. D12, 1219 (1975), and the $\bar{p}$n data are from A. Fridman et al, Phys. Rev. D12, 3414 (1975).

37. J. Elliott et al, Phys. Rev. Letters 34, 607 (1975).

38. Z. Koba, H. Nielsen and P. Olesen, Nucl. Phys. B40, 317 (1972).

39. T. Ferbel, Phys. Rev. D7, 925 (1973).

40. I wish to thank J. Whitmore for providing me with as yet unpublished results from the latest exposures at the 30-inch bubble chamber.

41. K. Moffeit et al, Phys. Rev. D5, 1603 (1972).

42. C. Bromberg et al, Nucl. Phys. B107, 82 (1976).

43. This effect has been discussed previously in R. Schindler et al, Phys. Rev. Letters 33, 862 (1974).

44. Reference (5) and P. Bosetti et al, Nucl. Phys. B54, 141 (1973).

45. T. Ferbel, Phys. Rev. D8, 2321 (1973).

46. C. Quigg and E. Rabinovici, Phys. Rev. D13, 2525 (1976). The parameterization used by Whitmore for the cross sections are:

$\sigma(\pi N) = (15.18\ \text{mb})p_{LAB}^{0.0755}$, $\sigma(KN) = (13.09\ \text{mb})p_{LAB}^{0.0755}$, $\sigma(NN) = (25.33\ \text{mb})p_{LAB}^{0.0755}$.

47. It is uncertain, for example, how the latest parameterization of the Pomeranchukon contribution to total cross sections by Quigg and Rabinovici affects the asymptotic form of the theoretical expression for $\langle n_c \rangle$. Preliminary indications are that $\langle n_c \rangle$ will rise more rapidly than that indicated by the B ℓn s rise in Table I.

48. J. Whitmore et al, Phys. Lett. 60B, 211 (1976).

49. Chan, H-M., Hsue, C.S., Quigg, C. and Wang J-M, Phys. Rev. Letts. 26, 672 (1971).

50. E.W. Beier et al, University of Pennsylvania preprint, submitted to the Tbilisi Meeting.

51. R.L. Anderson et al, Inclusive Hadron Exchange Scattering at 50-175 GeV. I thank D. Ritson for providing me an early version of the preprint.

52. A. Krzywicki and D. Weingarten, Phys. Lett. 50B, 265 (1974).

53. J. Derré et al, French-Soviet Collaboration, preprint M-12 (1974); C. Bromberg et al, Phys. Rev. D12, 1224 (1975); D. Fong et al, Phys. Lett. 61B, 99 (1976); J. Lamsa et al, Phys. Rev. Lett. 37, 73 (1976).

54. D. Weingarten et al, Rochester-ISU-MSU-ANL-FNAL-Maryland Preprint (1976).

55. J.P. DeBrion et al, Phys. Rev. Letts. 34, 910 (1975).

56. J.P. DeBrion et al, Phys. Letters. 52B, 477 (1974).

57. P. Stix et al, Rochester Report (in preparation).

58. See the lecture of A.J.S. Smith in this volume for an interesting comparison of the latest results for $\langle p_t \rangle$ of $\mu^+\mu^-$ pairs produced in hadronic collisions as a function of the mass of the $\mu^+\mu^-$ system. It appears that $\langle p_t \rangle$ for $\mu^+\mu^-$ pairs is larger than for produced hadrons of equivalent invariant mass.